Formation of CV chondrules by recycling of amoeboid olivine aggregate-like precursors

Yves Marrocchi, Romain Euverte, Johan Villeneuve, Valentina Batanova, Benoît Welsch, Ludovic Ferrière, Emmanuel Jacquet

Formation of CV chondrules by recycling of amoeboid olivine aggregate-like precursors

Yves Marrocchi [a,*], Romain Euverte [a,b], Johan Villeneuve [a], Valentina Batanova [c], Benoit Welsch [d], Ludovic Ferrière [e], Emmanuel Jacquet [f]

[a] *CRPG, CNRS, Université de Lorraine, UMR 7358, Vandoeuvre-lès-Nancy 54501, France*
[b] *LSCE, CNRS, UMR 8212, Gif-sur-Yvette 91198, France*
[c] *Université Grenoble Alpes, ISTerre, CNRS, UMR 5275, Grenoble 38000, France*
[d] *Department of Geology and Geophysics, University of Hawaii-Manoa, 1680 East-West Road, Honolulu, HI 96822, USA*
[e] *Natural History Museum, Burgring 7, A-1010 Vienna, Austria*
[f] *IMPMC, CNRS & Muséum national d'Histoire naturelle, UMR 7590, CP52, 57 rue Cuvier, 75005 Paris, France*

Abstract

We have studied porphyritic olivine-rich chondrules of the carbonaceous chondrite Kaba (CV3) by combined high-resolution X-ray mapping, quantitative electron microprobe analyses, and oxygen isotopic analyses *via* secondary ion mass spectrometry. These chondrules contain smaller inner-chondrule olivine grains characterized by low refractory element (Ca, Al, Ti) contents, and larger outer-chondrule olivine crystals that are enriched in refractory elements and show complex Ti and Al oscillatory zonings. Our O isotopic survey revealed that many of the inner-chondrule olivines are ^{16}O-richer than the relatively isotopically uniform outer-chondrule olivines. Inner-chondrule olivine crystals—only a minority of which may be derived from earlier generations of chondrules—are likely mostly inherited from nebular condensates similar to AOAs, as they share similar isotopic and chemical features and are thus interpreted as relict grains. Still, being ^{16}O-poorer than most AOAs, they may have experienced significant exchange with a ^{16}O-poor reservoir *prior* to chondrule formation (even if to a lesser degree than relicts in CM2 and ungrouped C2 chondrites). Subsequent incomplete melting of the relict grains produced Ca-Al-Ti-rich melts that engulfed the remaining relict olivine grains. The complex Ti and Al zoning patterns in outer chondrule (host) olivines, in particular the systematic dilution near the margin, seem to reflect gas-melt interactions (with e.g. SiO (g), Mg (g)) which also buffered the O isotopic composition of chondrule hosts. Together, these results demonstrate that important episodes of recycling of nebular condensates occurred in the solar protoplanetary disk.

Keywords: Chondrule; Oxygen isotopes; Relict olivine; Epitaxial growth; Gas–melt interactions

1. INTRODUCTION

Models of the evolution of the solar protoplanetary disk (hereafter SPD) must account for the physical and chemical processes that formed refractory inclusions and chondrules, the building blocks of primitive meteorites (chondrites). Thermodynamic calculations suggest that refractory inclusions condensed from a gas of solar composition, with calcium-aluminum-rich inclusions (CAIs) being the first condensates followed by amoeboid olivine aggregates (AOAs; Ebel, 2006; Komatsu et al., 2018). Chondrules, sub-millimeter-size silicate spheroids comprising olivine ($[Mg,Fe]_2SiO_4$) and low-Ca pyroxene ($[Mg,Fe]SiO_3$) crystals embedded in glassy mesostasis, constitute the main

* Corresponding author.
E-mail address: yvesm@crpg.cnrs-nancy.fr (Y. Marrocchi).

high-temperature component of chondrites (Scott and Krot, 2014). They formed by the solidification of melt droplets, though the mechanism(s) that produced those droplets remain(s) elusive (Hewins et al., 2005; Connolly and Jones, 2016). Refractory inclusions and chondrules experienced complex high-temperature histories before their incorporation into chondritic parent bodies, and thus provide key constraints on the evolving physicochemical conditions of the SPD (Russell et al., 2005).

Although there is a consensus that refractory inclusions and chondrules formed under different physicochemical conditions, it remains unclear whether they share a genetic relationship. Although petrographically recognizable relict refractory inclusions are rare in chondrules (e.g., Krot et al., 2007), REE patterns reminiscent of them are not uncommon (Jacquet and Marrocchi, 2017), and individual relict olivine grains that may have derived from AOAs have been occasionally reported in chondrules (Yurimoto and Wasson, 2002; Cohen et al., 2004; Russell et al., 2005; Ruzicka et al., 2012; Jacquet and Marrocchi, 2017; Marrocchi et al., 2018a; Schrader et al., 2018). However, such relicts may also be remnants of previous generations of chondrules (Ruzicka et al., 2007), or even debris from the mantles of early differentiated planetesimals, as envisioned by Libourel and Krot (2007) for granoblastic olivine aggregates (but see Whattam et al., 2008; Whattam and Hewins, 2009; Schrader et al., 2014; Marrocchi et al., 2018a). The difficulty in evaluating the relict record is that relict olivine grains are not easily recognizable, unless they record oxygen fugacities very different from their *in situ* host crystals and only recently have oxygen isotopic measurements allowed any distinction on the basis of their deviation from the host composition (Jones et al., 2004; Rudraswami et al., 2011; Ushikubo et al., 2012; Schrader et al., 2013; Tenner et al., 2013, 2015; Marrocchi and Chaussidon, 2015; Marrocchi et al., 2016; Jacquet and Marrocchi, 2017; Schrader et al., 2017, 2018; Hertwig et al., 2018; Chaumard et al., 2018; Marrocchi et al., 2018a).

A new analytical approach based on high-current X-rays maps has revealed previously unrecognized internal structures within three olivine-rich chondrules in chondrite Northwest Africa 5958 (NWA 5958, C2-ung; Jacquet et al., 2016), with Al-Ti-poor olivine cores surrounded by Al-Ti-rich olivine overgrowths (Marrocchi et al., 2018a). Oxygen isotopic measurements by secondary ion mass spectrometry (SIMS) demonstrate that many of these grains are isotopically distinct from their hosts and must be relict, allowing for the first time the *chemical* characterization of relict olivine grains (Marrocchi et al., 2018a). The latter and O isotopic compositions (despite their variability) indicate similarities with AOAs (Marrocchi et al., 2018a). Thus, chondrules are complex objects composed of (i) relict olivine grains inherited from an early generation of solids formed in the SPD, and (ii) host minerals that crystallized *in situ*, with significant gas-melt interactions in the chondrule-forming region(s) (Tissandier et al., 2002; Hezel et al., 2006; Libourel et al., 2006; Marrocchi and Libourel, 2013; Friend et al., 2016; Piani et al., 2016). In this model, relict grains are thus direct proxies of the first solids formed in the SPD, whereas host chondrule crystals represent thermochemical and isotopic sensors of the surrounding gas during chondrule formation. At the same time, (Libourel and Portail, 2018) interpreted type I chondrule cathodoluminescence zoning patterns similar to ours in X-ray maps as the result of crystallization from Ca-Al-rich melts produced in dense environments of the SPD. Clearly, the study of such zonings is nascent and will provide valuable insights into chondrule formation.

Here, following our proof-of-concept study on three NWA 5958 chondrules (Marrocchi et al., 2018a), we investigate a larger suite of olivine-rich type I chondrules in the weakly metamorphosed CV3 (OxB) chondrite Kaba (3.1–3.4; Bonal et al., 2006). As the CV group is the richest in refractory inclusions among chondrites (Ebel et al., 2016), our sample suite allows us to assess whether the relict grains therein show a stronger kinship to refractory inclusions or host olivines. The coupled chemical and isotopic analyses reported herein are examined in conjunction with literature data to define the chemical and oxygen isotopic characteristics of relict and host olivine grains in type I chondrules for the first time and in a statistically significant way.

2. MATERIAL AND METHODS

We surveyed all type I chondrules in two thin sections of Kaba (N4075 and O229 from the National History Museum, Vienna, Austria). Chondrules were examined microscopically in transmitted and reflected light. Scanning electron microscope observations were performed at CRPG-CNRS (Nancy, France) using a JEOL JSM-6510 with 3 nA primary beam at 15 kV. Among 66 Mg-rich porphyritic type I chondrules examined in the two sections, we selected six olivine-rich chondrules (e.g., Figs. 1 and 2) with crystals large enough to accommodate major, minor, and trace element and O isotopic analyses. High-resolution X-ray element distribution maps were performed at the Institut des Sciences de la Terre, (ISTerre, Grenoble, France) using a JEOL JXA-8230 electron microprobe analyzer (EMPA) equipped with five wavelength-dispersive spectrometers (WDS) and one silicon drift detector energy-dispersive spectrometer (EDS; Batanova et al., 2015). X-ray mapping was performed with an acceleration voltage of 20 kV, beam current of 500 nA, 1.5 μm step size, and dwell time of 500 ms. Al, Ca, Cr, Mn, and Ti were measured on the WDS detectors while Fe, Si, and Mg were measured on the EDS. The detection limits, estimated as the minimum difference between the average concentrations of visually distinct homogeneous zones as well as the standard deviation of the mean concentration of homogeneous zones, are below 40 ppm for Al, Ca, Ti, Cr, and Mn. These X-ray maps are semi-quantitative, as the background was not quantified by performing similar off-peak maps. Therefore, quantitative analyses of all olivine grains large enough to be isotopically characterized by SIMS were performed using a CAMECA SX-100 electron microprobe (CAMECA, Paris, France) at the University of Paris VI. The microprobe was calibrated using the following natural and synthetic standards for silicate analyses: diopside (Si, Ca, Mg), orthoclase (Al), MnTiO, (Mn, Ti), Cr_2O_3 (Cr), and Fe_2O_3 (Fe). A 60 nA focused beam, accelerated to

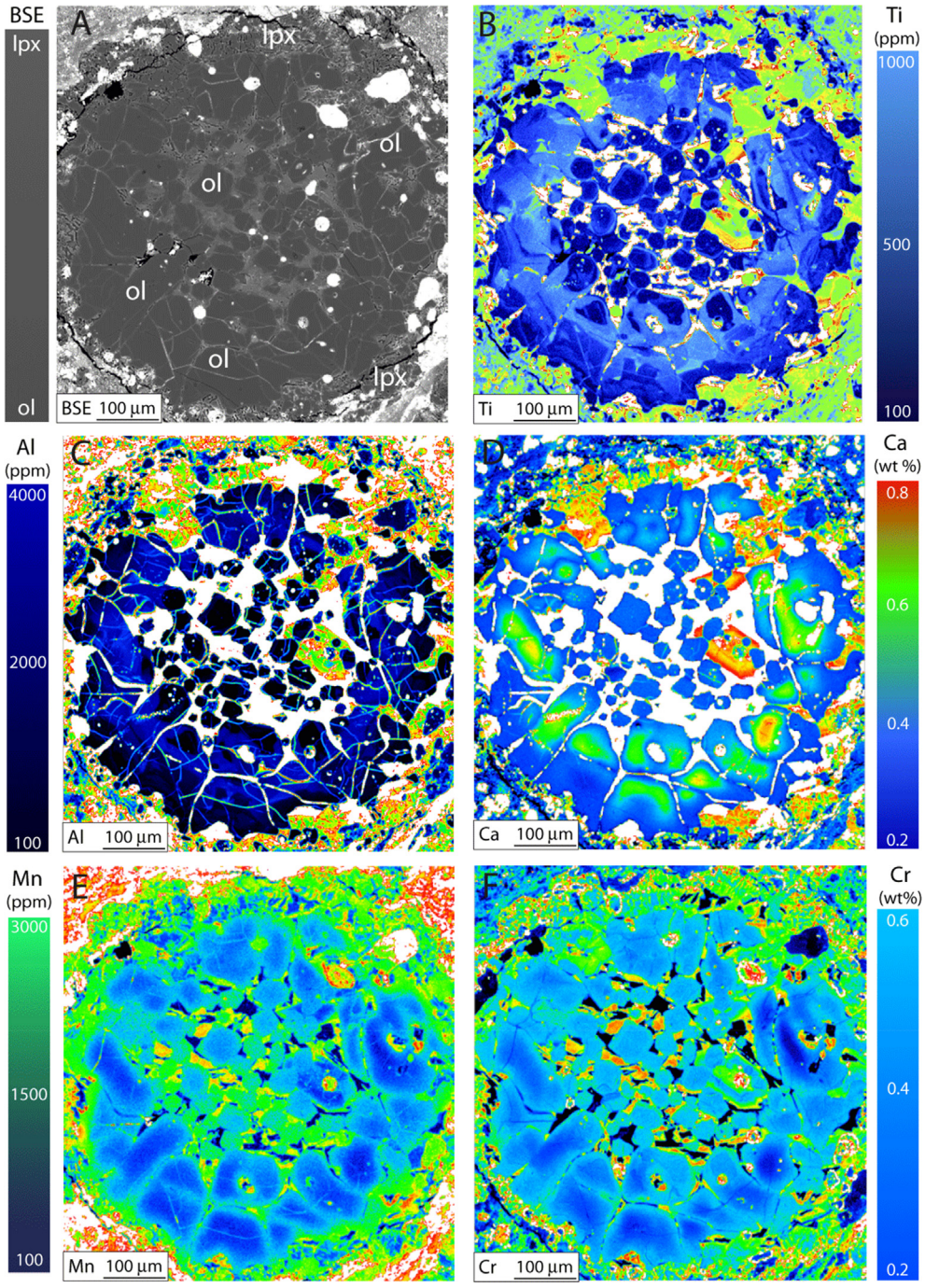

Fig. 1. (A) Back-scattered electron image of olivine-rich chondrule Ch-11 in CV3 chondrite Kaba (section N4075). (B) X-ray map of Ti distribution, revealing internal structures and emphasizing that chondrules are radially zoned with outer Ti-rich olivine grains and interiors dominated by smaller Ti-poor olivine grains surrounded by mesostasis. Ti-rich overgrowths commonly armor Ti-poor olivine cores. (C) to (F) Al, Ca, Mn, and Cr X-ray maps.

15 kV potential difference, was used for spot analyses of olivine with 20 s analysis times. Such a high current allowed detection limits of 150 ppm for Al, Ca, and Ti, 200 ppm for Mn and Si, and 400 ppm for Cr, Fe, and Mg. The PAP software was used for matrix corrections.

We measured the oxygen isotopic compositions of chemically characterized olivine crystals with a CAMECA ims 1270 E7 at CRPG-CNRS. $^{16}O^-$, $^{17}O^-$, and $^{18}O^-$ ions produced by a Cs^+ primary ion beam (~15 µm, ~4 nA) were measured in multi-collection mode with two off-axis Faraday cups (FCs) for $^{16,18}O^-$ and the axial FC for $^{17}O^-$. To remove $^{16}OH^-$ interference on the $^{17}O^-$ peak and to maximize the flatness atop the $^{16}O^-$ and $^{18}O^-$ peaks, the entrance and exit slits of the central FC were adjusted to

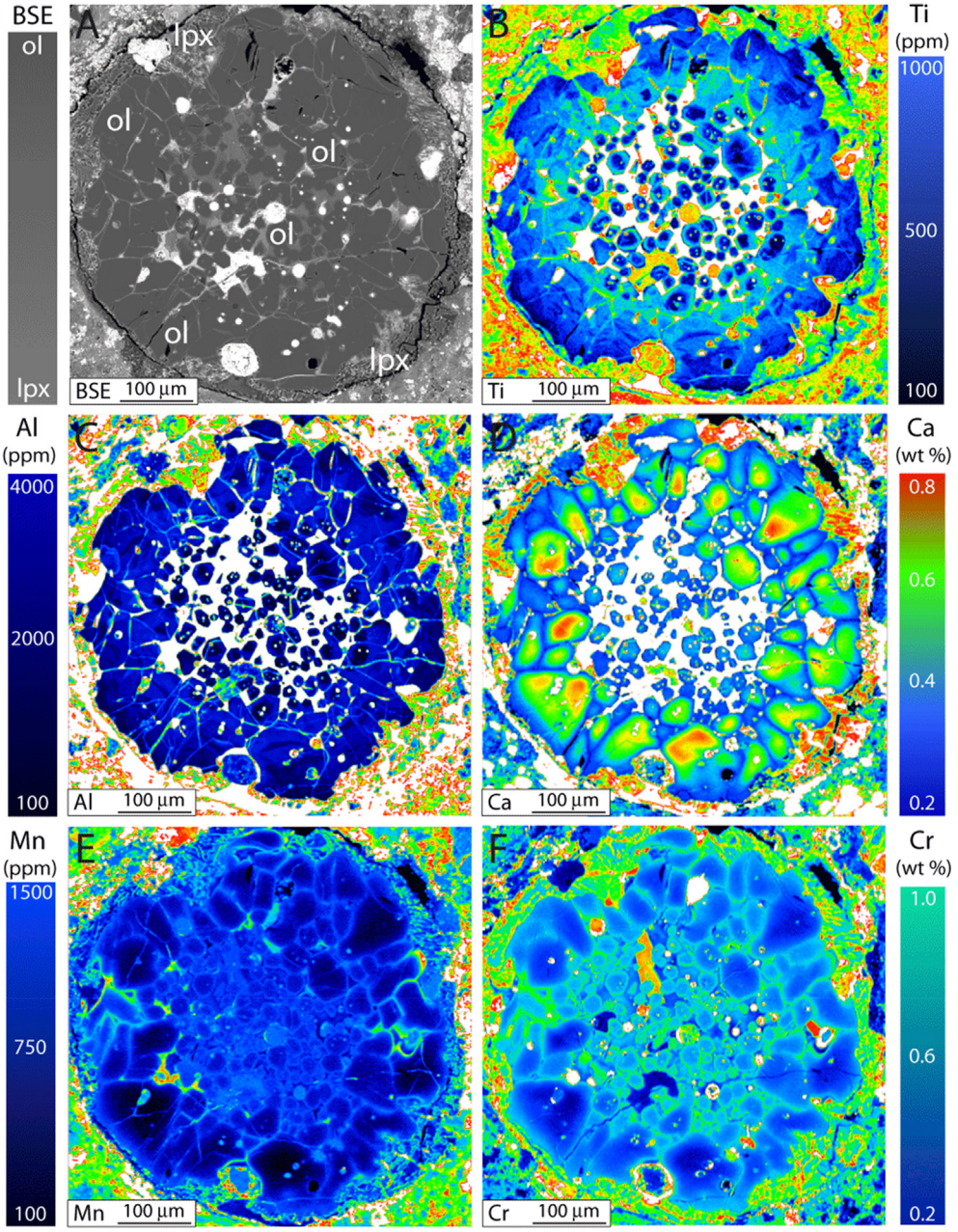

Fig. 2. (A) Back-scattered electron image of olivine-rich chondrule Ch-1 (Kaba, section O229). (B)–(F) Ti, Al, Ca, Mn, and Cr X-ray maps, as in Fig. 1.

obtain mass resolution power (MRP) of ~7000 for $^{17}O^{-}$. The multi-collection FCs were set on slit 1 (MRP = 2500). Total measurement times were 240 s (180 s measurement + 60 s pre-sputtering). We used three terrestrial standard materials (San Carlos olivine, magnetite, and diopside) to define the instrumental mass fractionation line for the three oxygen isotopes and correct for instrumental mass fractionation due to the matrix effect of olivine. To obtain good precision on analytical measurements, we analyzed, in order, four standards, eight chondrule olivine crystals, and four standards. Typical count rates obtained on the San Carlos olivine standards were 2.5×10^9 cps for ^{16}O, 1.0×10^6 cps for ^{17}O, and 5.4×10^6 cps for ^{18}O. Between 20 and 46 O isotopic measurements were performed on Mg-rich olivine crystals in each chondrule, with typical uncertainties of 0.2, 0.4, and 0.9‰ for $\delta^{18}O$, $\delta^{17}O$, and $\Delta^{17}O$ ($=\delta^{17}O - 0.52 \times \delta^{18}O$), respectively (Table 1). The error on $\Delta^{17}O$ was calculated by quadratically summing the errors on $\delta^{17}O$ and $\delta^{18}O$ and the standard deviation of $\Delta^{17}O$ values of the four terrestrial standards. All the SIMS spots were carefully checked by SEM and those that were close to fractures, near Fe-Ni metal beads or not completely in olivine grains were excluded.

Table 1
Oxygen isotopic compositions of host and relict olivine grains in chondrules of chondrite Kaba. Relict grains correspond to those with low Ti contents and $\Delta^{17}O$ values outside 3σ of the average homogenous chondrule phase $\Delta^{17}O$ value (Ushikubo et al., 2012).

Chondrite	Chondrule #	*Olivine type*	n	$\delta^{18}O$	2σ	$\delta^{17}O$	2σ	$\Delta^{17}O$	2σ
Kaba-N4075	Ch-11	Host	43	−7.3	0.2	−10.4	0.4	−6.6	0.5
		Relict		−18.7	0.3	−20.9	0.5	−11.2	0.8
		Relict		−13.1	0.2	−16.0	0.5	−9.2	1.1
		Relict		−15.6	0.2	−17.9	0.4	−9.8	1.0
		Relict		−12.1	0.2	−15.0	0.4	−8.6	0.9
		Relict		−10.9	0.2	−14.4	0.4	−8.7	1.0
Kaba-N4075	Ch-25	Host	11	1.4	0.2	−2.0	0.4	−2.7	0.4
		Relict		−22.0	0.2	−24.7	0.4	−13.3	1.0
		Relict		−9.8	0.2	−13.1	0.4	−8.0	0.9
		Relict		−5.2	0.2	−8.9	0.4	−6.2	1.0
		Relict		−4.4	0.2	−7.3	0.5	−5.0	1.1
		Relict		−3.7	0.2	−7.5	0.5	−5.6	1.2
		Relict		−24.2	0.2	−27.4	0.4	−14.8	1.0
		Relict		−18.2	0.2	−21.5	0.4	−12.0	1.0
		Relict		−0.6	0.2	−4.8	0.4	−4.4	1.0
		Relict		−44.6	0.2	−46.1	0.3	−23.0	0.9
Kaba-N4075	Ch-1	Host	43	−3.9	0.7	−7.1	0.5	−5.1	0.9
Kaba-N4075	Ch-18	Host	8	4.9	0.4	2.6	0.6	0.0	0.4
		Relict		−27.3	0.3	−29.8	0.6	−15.6	1.1
		Relict		−0.2	0.2	−2.3	0.4	−2.2	1.0
Kaba-N4075	Ch-12	Host	37	−4.9	1.3	−8.0	1.3	−5.5	0.7
Kaba-0229	Ch-1	Host	38	−4.0	0.2	−7.6	0.4	−5.6	0.6
		Relict		−14.8	0.2	−17.3	0.4	−9.6	1.0
		Relict		−20.5	0.3	−24.1	0.6	−13.4	1.1
		Relict		−15.8	0.2	−19.1	0.4	−10.8	1.0
		Relict		−30.9	0.2	−34.2	0.4	−18.1	1.0
		Relict		−40.6	0.2	−43.1	0.3	−23.0	0.9

3. RESULTS

The six selected olivine-rich type I porphyritic chondrules are characterized by olivine crystals with different sizes. Small (~30–60 μm), rounded to subhedral olivine grains are present in chondrule interiors whereas larger grains (~80–200 μm) are located in the outer zone of chondrules (Figs. 1A, 2A and S1). Chondrule rims are dominated by low-Ca pyroxenes oriented parallel to the chondrule surface, with resorbed or poikilitically enclosed olivines (Figs. 1A, 2A). Chondrule olivines appear homogeneous in backscatter intensity (Figs. 1A, 2A) and major element composition ($Fo_{98.6\pm0.2}$; Table S1), but X-ray maps reveal that the small inner-chondrule olivine grains often have Ti-Al-depleted cores and Cr-Mn-enriched rims (Figs. 1 and 2, Table S1). Some lack Ti-Al-rich margins altogether and/or may be uniformly Cr-Mn-enriched (Figs. 1 and 2). Ca shows little zoning, if not a faint *reverse* one, in these interior grains (Figs. 1 and 2; see also Jacquet and Marrocchi, 2017). Outer-chondrule olivine crystals (termed "palisadic" by Libourel and Portail, 2018) have the maximum Ca, Al, and Ti contents of the chondrule in their interiors, but those contents decrease as Mn content increases toward the crystal edge. Whereas the Ca and Mn zonings are smooth (decreasing from 0.5 to 0.15 wt% and increasing from 0.03 to 0.9 wt%, respectively, from core to rim), Ti and Al zonings are oscillatory (possibly in a more pronounced way for Ti) with periods of 5–20 μm, ranging from 200–1500 ppm Ti and 250–4000 ppm Al (Fig. 3, Table S1). Such oscillatory zonings have previously been reported from cathodoluminescence maps (Steele et al., 1985; Steele, 1986, 1995; Libourel and Portail, 2018) and phosphorus X-ray maps (McCanta et al., 2016), and one Allan Hills A81189 (EH3) chondrule even showed strong Fo_{75-97} oscillations in its olivine phenocrysts (Lusby et al., 1987).

Olivine O isotope compositions define a very good correlation (Fig. 8A; $r^2 = 0.99$; MSWD = 9.5) along the primary chondrule minerals (PCM) line, with $\delta^{18}O$ and $\delta^{17}O$ values ranging from −44.6 to 5.8‰ and from −46.1 to 3.6‰, respectively, the heaviest values being similar to the terrestrial mantle, i.e., $\delta^{18}O = 5.8‰$ and $\delta^{17}O = 3.0‰$ (Figs. 4–7, Tables 1 and S1). This trend is also observed for other chondrules from Kaba (Hertwig et al., 2018), Murchison (Chaumard et al., 2018), NWA 5958 (Marrocchi et al., 2018a; Fig. 9A), CR and CO chondrites (Tenner et al., 2013, 2015, 2018; Schrader et al., 2013, 2014, 2017, 2018) and Acfer 094 (Ushikubo et al., 2012). Four chondrules show internal mass-independent O isotopic heterogeneity beyond analytical uncertainties, with $\Delta^{17}O$ values varying by >20‰ (Figs. 4–6, Table 1); the $\Delta^{17}O$ values of olivines within the other two chondrules are either indistinguishable or vary within a narrow range (Fig. 7, Table 1). As in our previous work (Marrocchi et al., 2018a), we adopt the convention of (Ushikubo

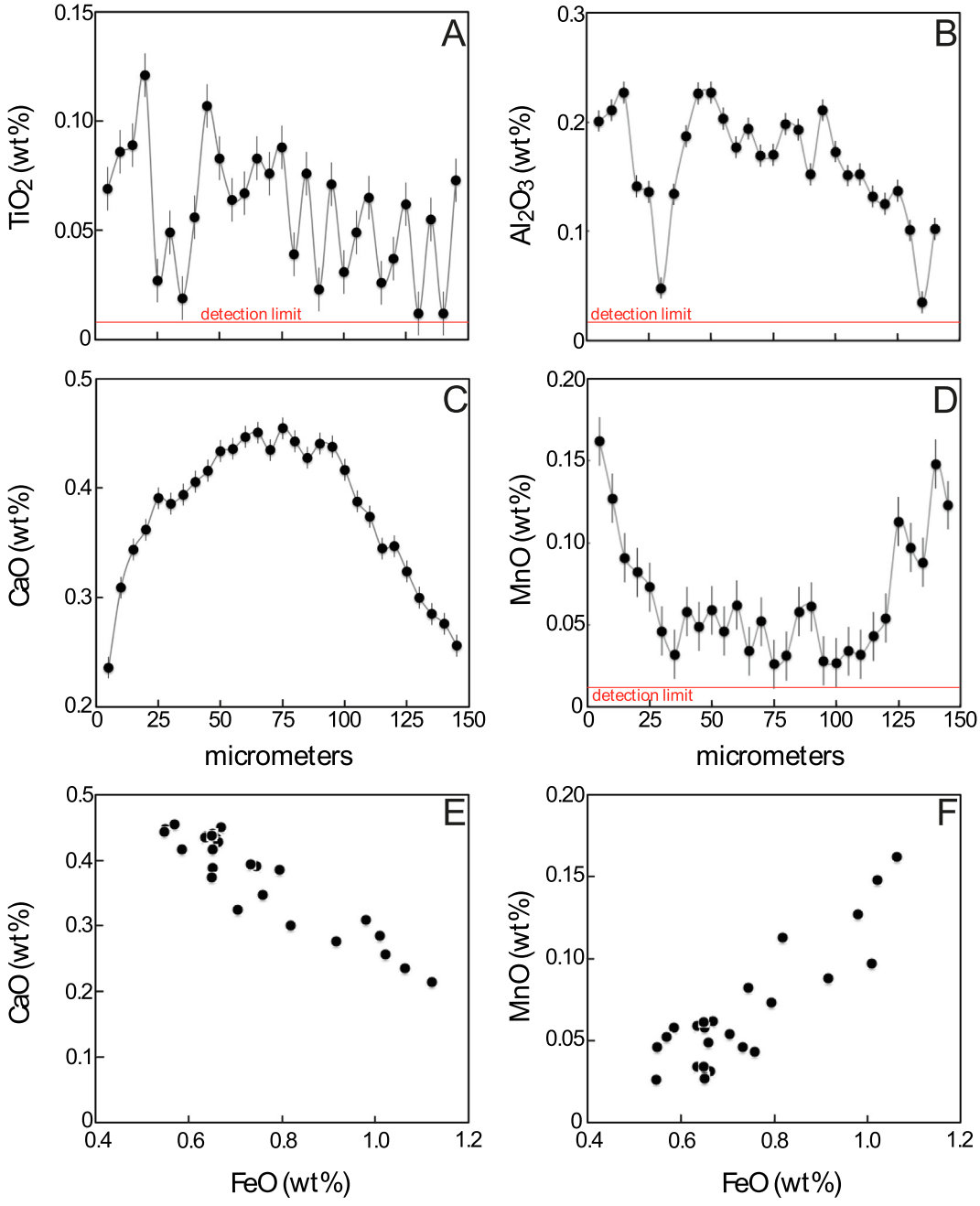

Fig 3. Profile measurements showing representative (A) TiO_2 and (B) Al_2O_3 oscillatory zonings and smooth (C) CaO and (D) MnO zoning patterns observed in large outer-chondrule olivine grains (data from chondrule Ch-26; Kaba, section N4075). Our data show (E) positive FeO-CaO and (F) negative FeO-MnO relationships within single olivine grains.

et al., 2012) and consider relict grains as those with $\Delta^{17}O$ values beyond 3σ of the host value. Unlike our study of NWA 5958 in which one chondrule showed ^{16}O-poor relicts (Marrocchi et al., 2018a), the relict olivine grains studied herein are always enriched in ^{16}O compared to their host (Figs. 4–11, Table S1). To some extent, this is a statistical fluctuation, as three of the eleven relict-bearing Kaba chondrules studied by (Hertwig et al., 2018) contained ^{16}O-poor relicts whereas (Chaumard et al., 2018) only found one such chondrule out of nine relict-bearing chondrules in Murchison (closely related to NWA 5958; Jacquet et al., 2016). Despite those variations, Kaba relicts extend to compositions richer in ^{16}O than those in NWA 5958 or Murchison (Figs. 9, 12; Hertwig et al., 2018; Chaumard et al., 2018; Marrocchi et al., 2018a).

As in our previous study (Marrocchi et al., 2018a), relicts are systematically found clustered in the chondrule interior and depleted in Ti, Al, and sometimes Ca, and enriched in Mn relative to host olivine crystals, which contain variable concentrations of these elements (Figs. 4–7). Depending on the chondrule, ^{16}O-rich olivines plot either in the upper or lower range of the Fo contents of the

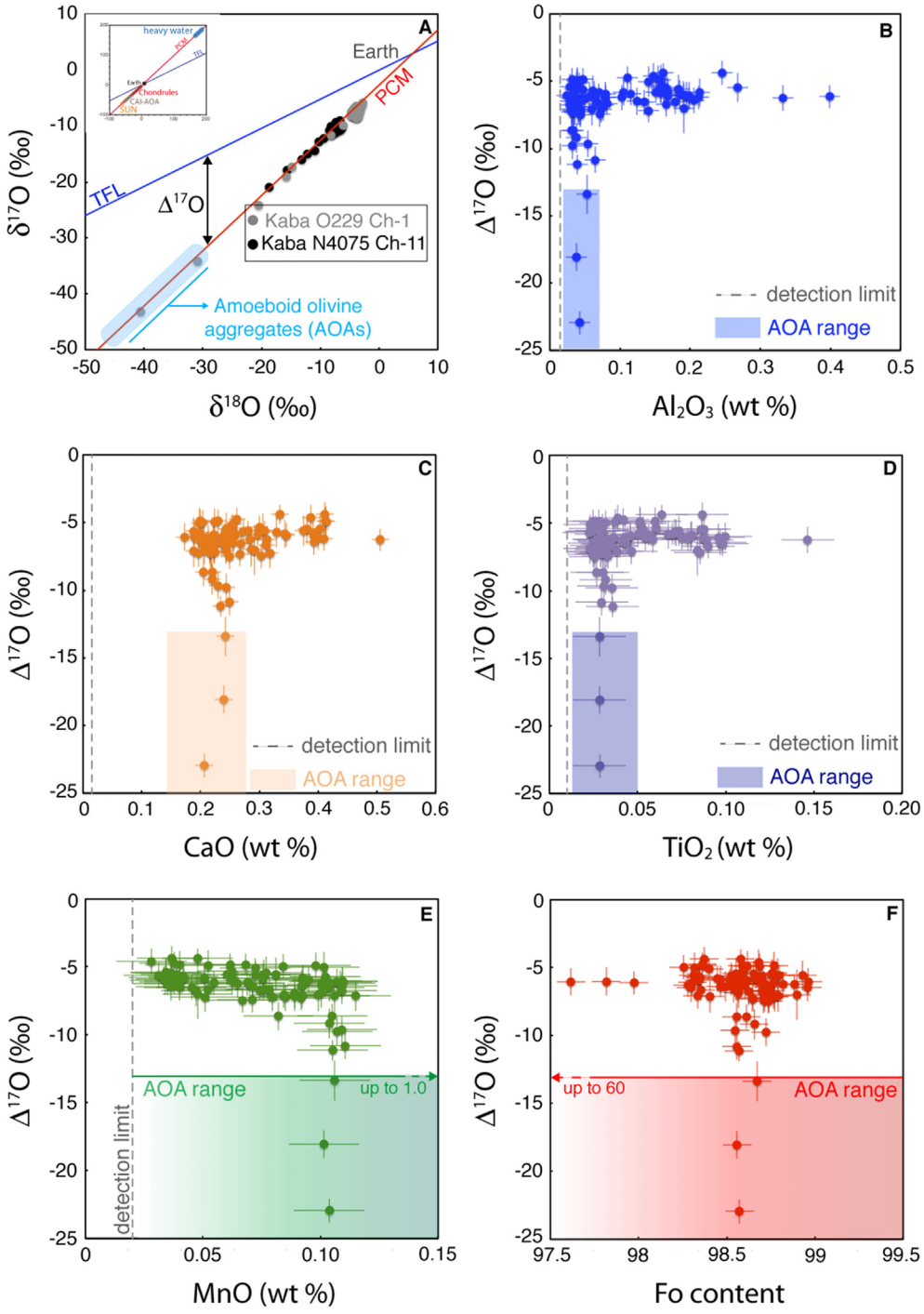

Fig. 4. (A) Oxygen isotopic compositions of olivine crystals within two chondrules of Kaba (Ch-11, section N4075, and Ch-1, section O229). The data show the presence of important mass-independent variations within each chondrule (up to 47‰), with the ^{16}O-enriched olivines having similar O isotopic compositions as AOA olivines (Krot et al., 2004). The Terrestrial Fractionation Line (TFL) and Primary Chondrule Minerals (PCM; (Ushikubo et al., 2012)) are shown for reference. Incompatible element concentrations plotted against O isotopic compositions (as Δ^{17}O) reveal that ^{16}O-rich olivines are systematically depleted in (B) Al, (C) Ca, and (D) Ti, and enriched in (E) Mn (E) to ^{17,18}O-rich olivines that show variable concentrations of those elements. (F) Fo content *vs.* Δ^{17}O values, showing that relict and host olivines have similar Fo contents.

Δ^{17}O-constant host olivines of the same chondrule (Figs. 4–7, Table S1). ^{16}O-rich olivines in Kaba, Murchison, and NWA 5958 generally plot within the fields defined by host olivines in minor element biplots (in particular the CaO vs. FeO non-monotonic trend characterized by a decrease then increase of CaO content with increasing FeO content; Fig. 11), but it is noteworthy that the most CaO-rich relict olivines are the most ^{16}O-poor (Fig. 10A). We do not

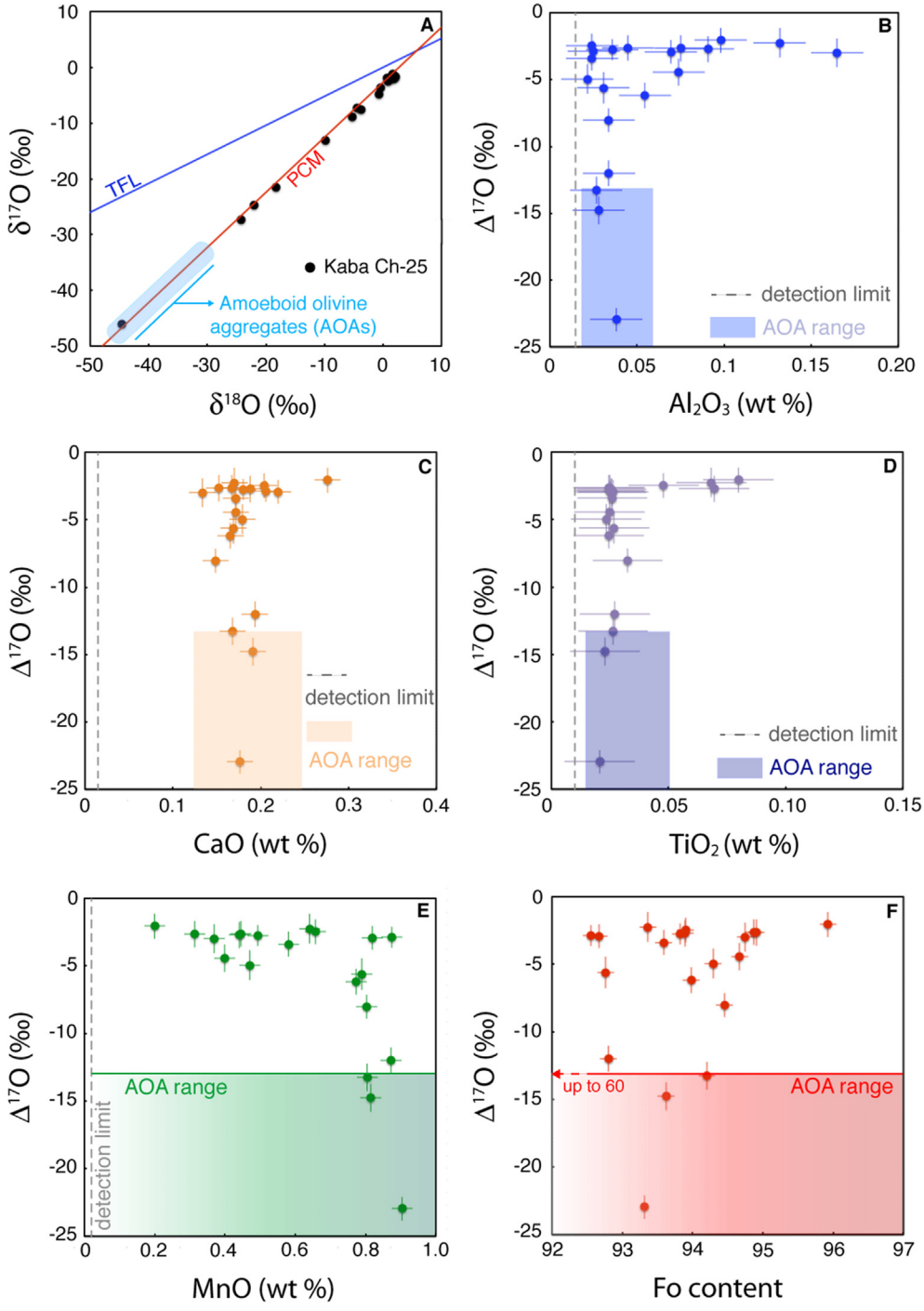

Fig. 5. Oxygen isotopic compositions and incompatible element concentrations of olivines within chondrule Ch-25 (Kaba, section N4075). See Fig. 4 for details.

observe a correlation between $\Delta^{17}O$ and relict olivine Fo contents: most cluster around 1 wt% FeO (Fig. 10b).

We note that in our comparison with the literature, we focused on recent data on the CV3 Kaba (Hertwig et al., 2018), CM2 Murchison (Chaumard et al., 2018), and the C2-ungrouped (if CM-related) NWA 5958 chondrites (Marrocchi et al., 2018a; Figs. 9–12). This is because precisely these publications allowed direct linking of minor element analyses to O isotopic compositions of the same olivine grains (as specifically investigated here), and addressed similar objects (type I porphyritic olivine-rich chondrules) in the same (or affiliated) chemical groups of chondrites as in our project. This however should not obscure the vastly greater body of studies which reported O isotopic compositions of chondrules of a wide range of types, as listed in the introduction, and which will feed into the ensuing discussion.

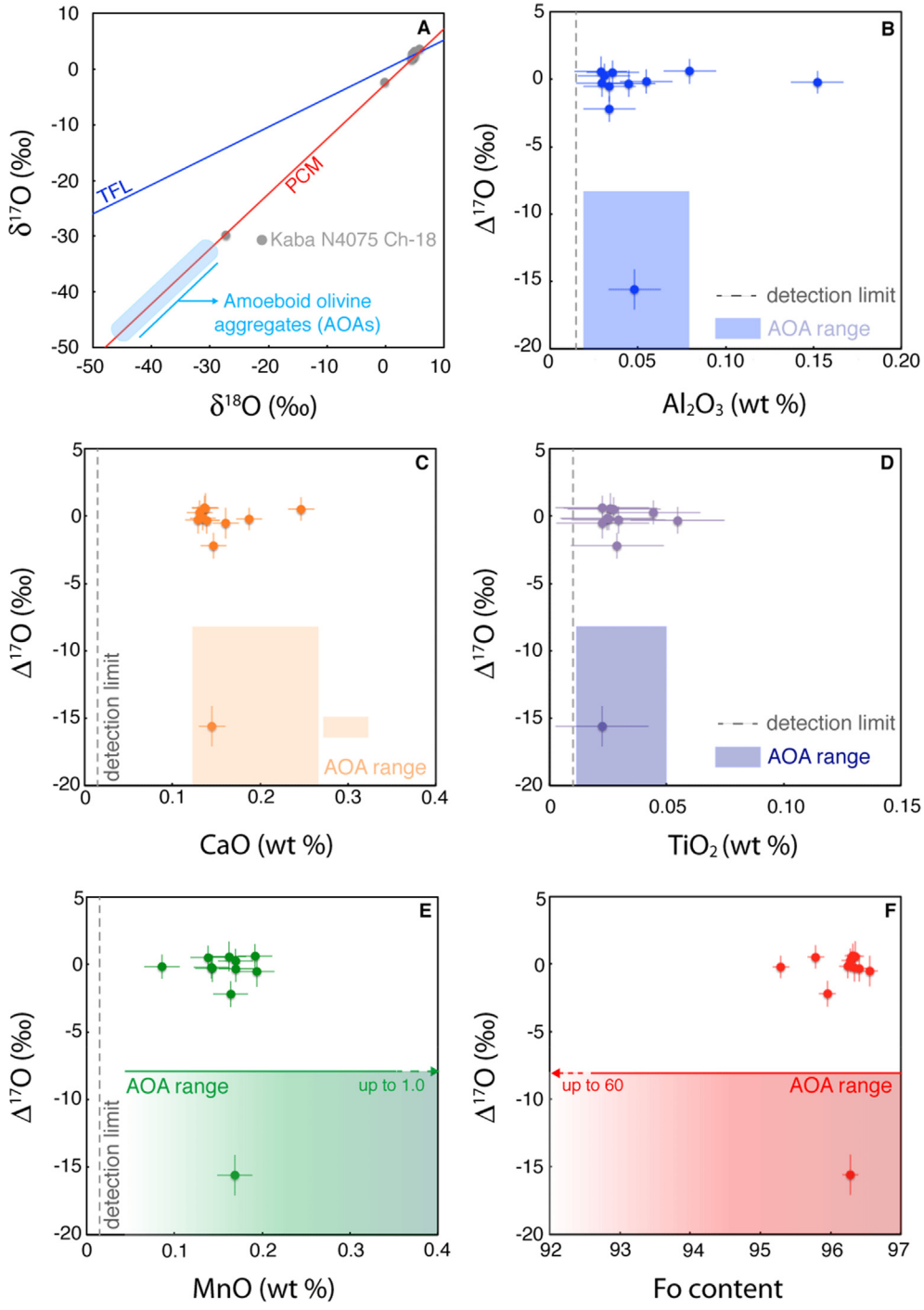

Fig. 6. Oxygen isotopic compositions and incompatible element concentrations of olivines within chondrule Ch-11 (Kaba, section N4075). See Fig. 4 for details.

4. DISCUSSION

4.1. Identification of relict olivine grains in chondrules

Our results reveal that some olivine grains in Kaba's chondrules have $\Delta^{17}O$ different from their host's, and their distinctive chemical signatures (Ca-Al-Ti depletion and Mn enrichment) are emphasized by our X-ray maps and EMPA analyses (Figs. 1, 2, 4–6, 11, Table S1). As in our previous work (Marrocchi et al., 2018a), we interpret these grains as relicts inherited from isotopically heterogeneous precursors, whereas host grains grew *in situ* during chondrule formation, with their O isotopic composition being buffered by interaction with the surrounding gases. However,

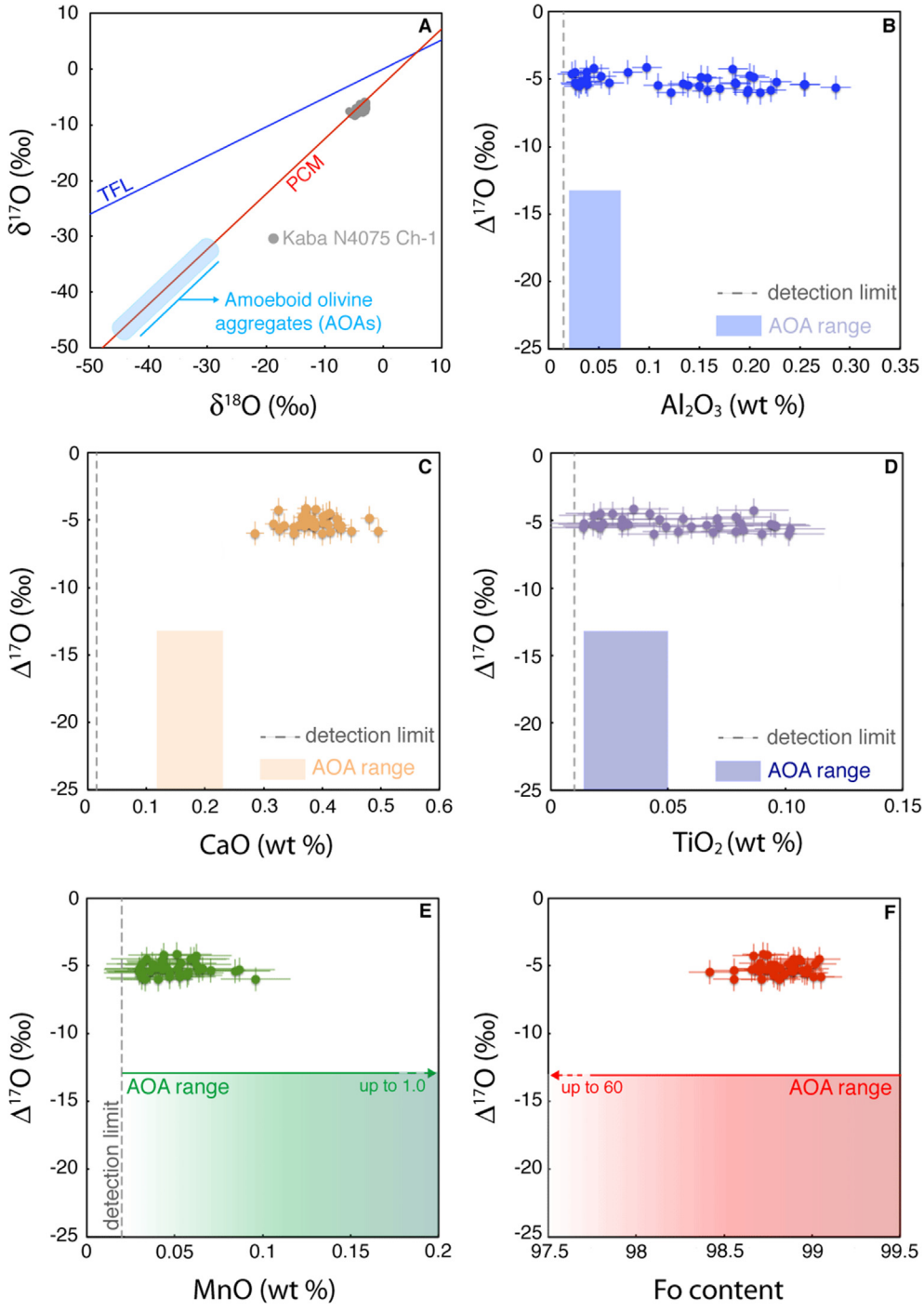

Fig. 7. Oxygen isotopic compositions and incompatible element concentrations of olivines within chondrule Ch-18 (Kaba, section N4075). See Fig. 4 for details.

Libourel and Portail (2018) interpreted similar cathodoluminescence zonings as resulting from the crystallization of refractory condensed melts that were progressively diluted by incoming gas from the SPD (see also Pack et al., 2004, 2005). In such a framework, olivine grains should exhibit a gradual Ca-Al-Ti depletion from the centers to the edges of chondrules, with the isotopic composition of the least refractory olivines uniformly buffered by the ambient gas, inconsistent with the chemical variations revealed by X-ray and cathodoluminescence maps and our SIMS analyses (Fig. 12; Pack et al., 2004, 2005; Libourel and Portail, 2018; Marrocchi et al., 2018a). Clearly, the isotopically distinct Ca-Al-Ti-poor grains must have formed earlier than their host grains.

Nonetheless, it is noteworthy that within each chondrule we analyzed (this work and Marrocchi et al. (2018a) relict

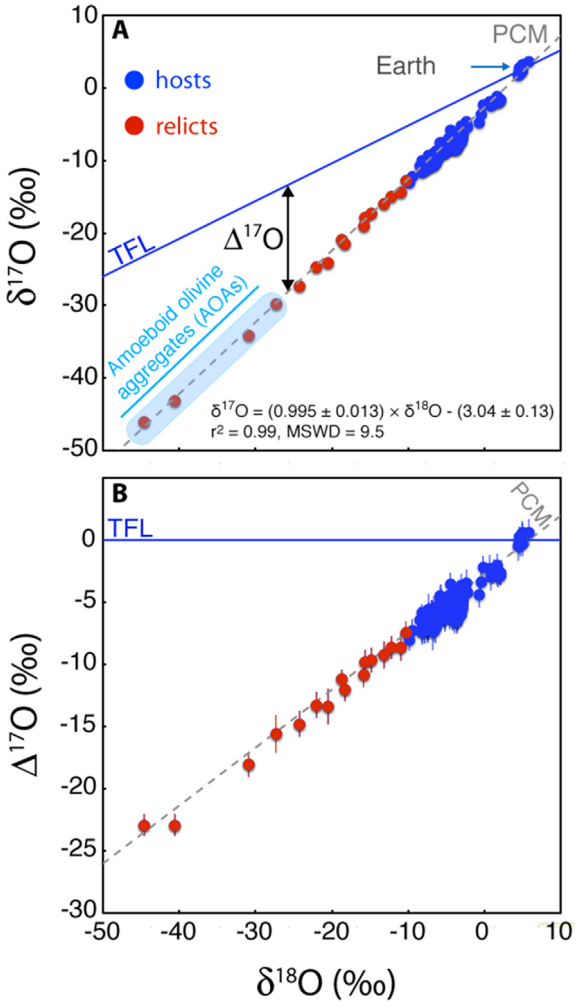

Fig. 8. (A) Oxygen three-isotope plot of all chondrule olivine crystals measured in this study. They plot along the PCM and define an isotopic continuum, suggesting several episodes of olivine crystallization. Relict olivine grains (red circles) are defined on the basis of their ^{16}O- and Mn-rich and Ti-Al-Ca-poor compositions; blue circles show host olivines. (B) $\Delta^{17}O$ vs. $\delta^{18}O$ values of all chondrule olivines measured in this study. Little variation is observed about the PCM, as expected for chondrule formation during nebular processes. (For interpretation of the references to color in this figure legend, the reader is referred to the web version of this article.)

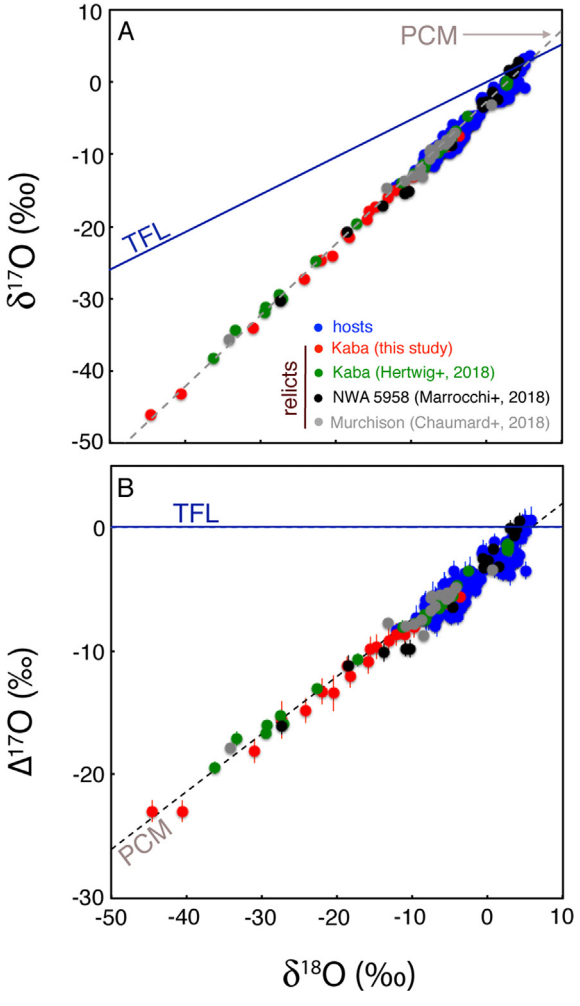

Fig. 9. (A) Oxygen isotopic compositions of host olivine grains (blue circles) and relict olivine grains from the CV chondrite Kaba (this study and Hertwig et al., 2018; red and green circles, respectively), the CM-related NWA 5958 (Marrocchi, Villeneuve, et al., 2018; black circles) and the CM chondrite Murchison ((Chaumard et al., 2018); gray circles). (B) $\Delta^{17}O$ vs. $\delta^{18}O$ values of host and relict olivine grains from the same meteorites. (For interpretation of the references to color in this figure legend, the reader is referred to the web version of this article.)

olivine grains are either enriched or depleted in ^{16}O relative to the host, but never both in the same chondrule (Figs. 4–11; Marrocchi et al., 2018a). At first glance, this runs counter to the expectation that the compositions of precursor grains of a given chondrule are independent from that of the ambient gas. This could warrant an alternative scenario of fractional crystallization where the "relicts" might represent the earliest crystals formed from chondrule melts whose O isotopic composition was evolving (via progressive isotopic equilibration with the SPD gas and/or evolution of the gas composition) from an initial composition approximated by the most extreme olivine O isotopic compositions observed toward that of the present-day host (Libourel and Portail, 2018). Subsequent crystallization of the residual melt would have produced olivine richer in incompatible Ca, Al, and Ti, with a then-fixed $\Delta^{17}O$ value. However, this scenario would not account for the sharp boundaries between Al-Ti-rich overgrowths and the Al-Ti-poor grains that they mantle (Figs. 1 and 2), at variance with the expected smooth normal zoning. Chondrules containing relict olivines with $\Delta^{17}O$ values both above and below those of the host have been reported, e.g., K18 in Kaba (Hertwig et al., 2018) and Y25 in Yamato 81020 (CO3.0; Tenner et al., 2013), as well as "heterogeneous chondrules" for which no host composition could be readily defined (e.g., Ushikubo et al., 2012; Schrader et al., 2013, 2018; Chaumard et al., 2018). The apparent rarity of such chondrules may be due to: (i) insufficient statistics of relict grains

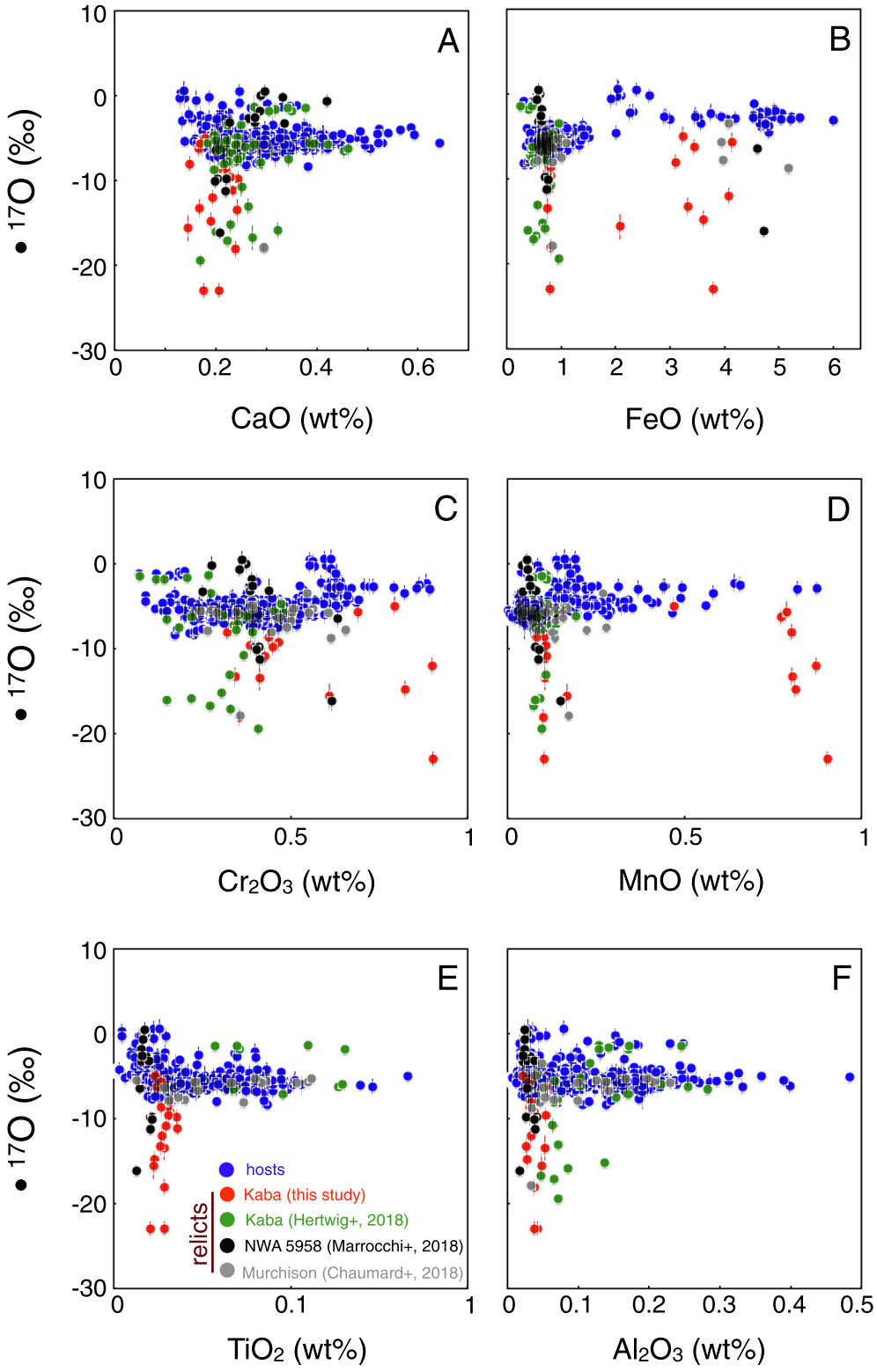

Fig. 10. Element concentrations plotted against $\Delta^{17}O$ reveal that relict olivine grains (red circles) are commonly depleted in (A) CaO, (B) FeO, (C) Cr_2O_3, (D) MnO, (E) TiO_2 and (C) Al_2O_3 relative to their host olivine crystals (blue circles), which are characterized by variable concentrations of these elements. (For interpretation of the references to color in this figure legend, the reader is referred to the web version of this article.)

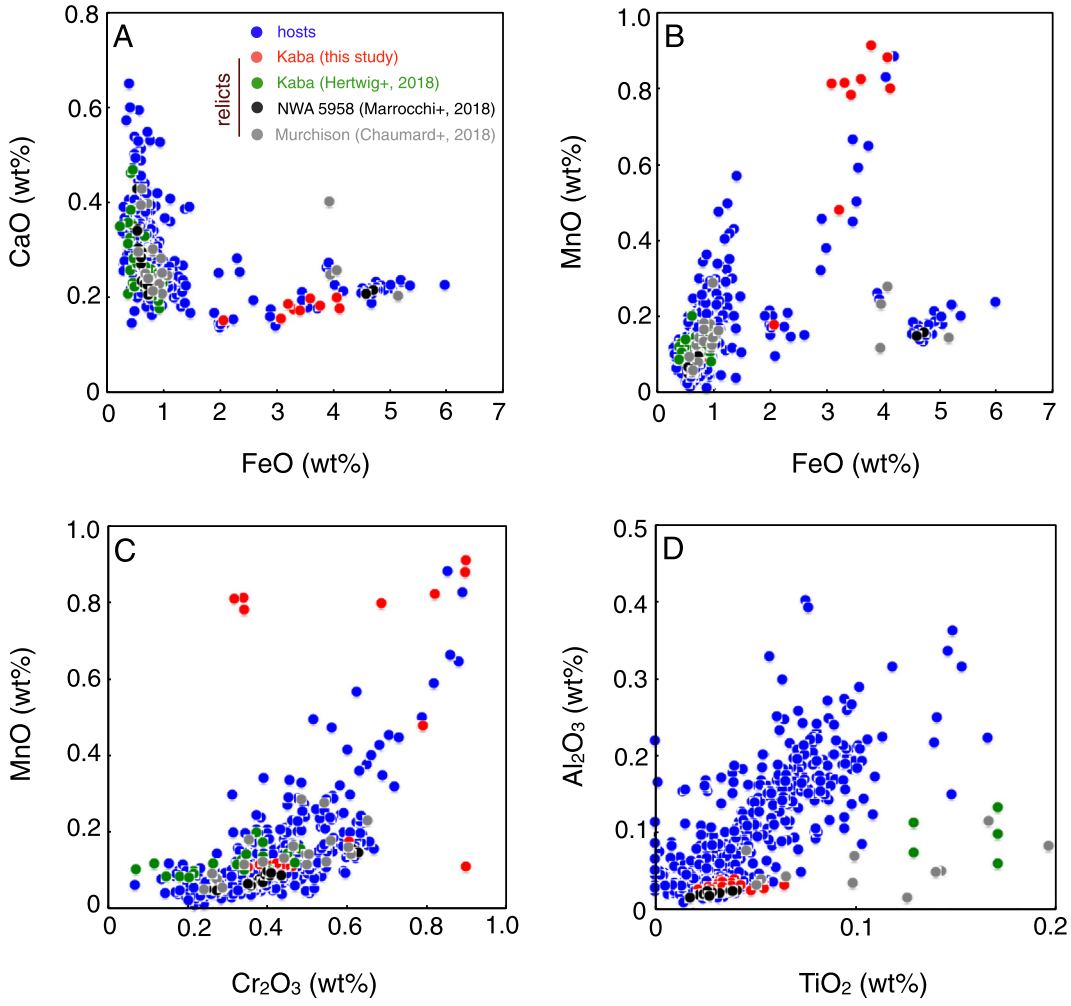

Fig. 11. (A) CaO vs. FeO concentrations in relict (red) and host (blue) olivine grains. (B) MnO vs. FeO concentrations in relict and host olivine grains. (C) MnO vs. Cr_2O_3 concentrations in relict and host olivine grains. (D) TiO_2 vs. Al_2O_3 concentrations in relict and host olivine grains. (For interpretation of the references to color in this figure legend, the reader is referred to the web version of this article.)

analyzed in individual chondrules in past studies; (ii) the high frequency of ^{16}O-rich compositions beyond the range of host values among relicts, which makes the presence of ^{16}O-poor relicts less likely; and/or (iii) some correlation between the compositions (and origins) of grains in a given chondrule precursor (as opposed to a completely random mechanical aggregate of grains of different nebular provenances), which increases the chances of clustering grains with compositions on one side of the future host composition.

We thus conclude that we have indeed identified relicts of solid precursors to chondrules that formed earlier during the history of the SPD and survived the chondrule-forming event(s). The metal blebs enclosed in relict olivines may therefore be inherited from their precursors (Marrocchi et al., 2018a) rather than seeds for olivine nucleation (Libourel and Portail, 2018). In that case, the paucity of metal grains in barred olivine chondrules may be rather an effect than a cause (Libourel and Portail, 2018) of their nature, in the sense that metal may have been lost from fully molten chondrules more easily than from incompletely molten ones, as suggested by the higher frequency of indentations in nonporphyritic chondrules (Gooding and Keil, 1981) which (Grossman and Wasson, 1985) ascribed to such fissions.

4.2. Nature and origin of relict grains

Several possibilities remain concerning the nature of solid chondrule precursors. We argued at length against a planetary origin in Marrocchi et al. (2018a), and Libourel and Portail (2018) relinquished a mantle origin for granoblastic olivine aggregates in favor of gas-assisted epitaxial growth, so we need not repeat this reasoning here (see also Schrader et al., 2014).

Some of the observed relicts could correspond to early generations of chondrules (e.g., Ruzicka et al., 2007; Schrader et al., 2018). Such an origin can only be considered for relicts with Δ^{17}O values similar to those of host olivines from other chondrules, provided the early generations of chondrules have not been entirely destroyed. If we consider that host olivine Δ^{17}O values are generally bracketed by the most extreme host compositions observed here, i.e., –8.38‰ and 0.6‰, this involves 25 of 48 relicts in

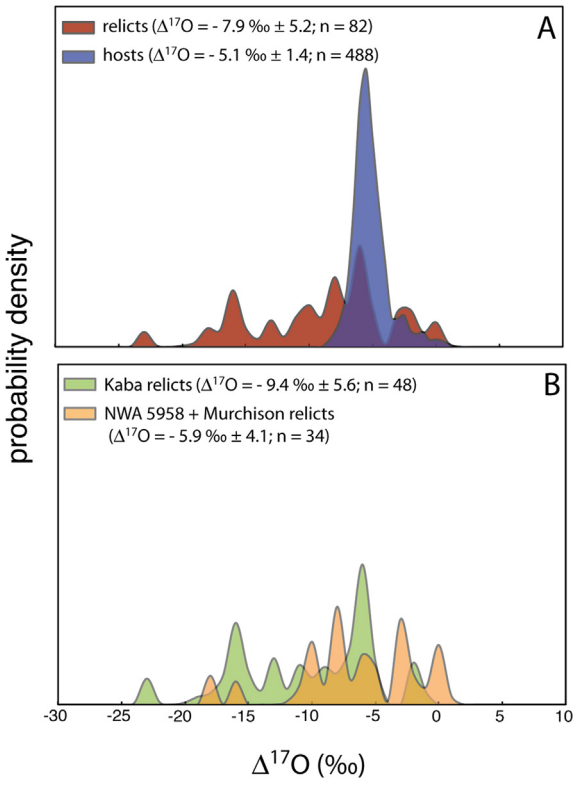

Fig. 12. Curves show probability density functions of $\Delta^{17}O$ of relict (red) and host (blue) olivine grains in our Kaba chondrules from this study and (Hertwig et al., 2018), NWA 5958 (Marrocchi et al., 2018a) and Murchison (Chaumard et al., 2018). The average, standard deviation and the number of data points in the distribution are given for both relict and host olivine grains.

Kaba (this study, Hertwig et al., 2018) and 29 of 37 relicts in NWA 5958 and Murchison (Chaumard et al., 2018; Marrocchi et al., 2018a). However, even those relicts are commonly Ca-Al-Ti-poor compared to the host (Fig. 10) and the most CaO-rich ones are the most ^{16}O-poor. This suggests that probably only a minority of those relicts were sourced from chondrules. In fact, this should be expected as the presence of matrix and refractory inclusions in CV chondrites indicates that chondrule-forming events were not so frequent as to convert more than a moderate fraction of precursors into chondrules, and *a fortiori* to operate twice on the same grains.

This argument can be made quantitative if we consider that the different chondrule-forming events experienced by a given grain of nebular matter were independent and rare. Then, the number n of chondrule-forming events experienced by one such grain obeys a Poisson distribution (Jacquet et al., 2015) of the form:

$$P(n) = e^{-\lambda}\frac{\lambda^n}{n!}, \quad (1)$$

where λ is the mean number of chondrule-forming events experienced by individual single grains. Since matrix-chondrule complementarity indicates that the modal composition of a carbonaceous chondrite is representative of its native reservoir (Jacquet et al., 2012), the chondrule ('chd') fraction of that reservoir is:

$$x_{\mathrm{chd}} = 1 - P(0) = 1 - e^{-\lambda} \quad (2)$$

Thus, the fraction of chondrule-hosted particles that have undergone at least two chondrule-forming events is:

$$f_{\mathrm{recycled}} = \frac{1 - P(0) - P(1)}{1 - P(0)} = 1 + \left(\frac{1}{x_{\mathrm{chd}}} - 1\right)\ln(1 - x_{\mathrm{chd}}) \quad (3)$$

Considering Kaba, if we take $x_{\mathrm{chd}} = 34.3 + 3.4 = 37.7\%$ from Zanda et al. (2006) (that is, counting as chondrules *sensu lato* the 3.4 vol% metal grains that are likely byproducts of chondrule formation and ignoring the density difference between matrix and chondrules; Jacquet et al., 2013; Campbell et al., 2005), we obtain $f_{\mathrm{recycled}} = 22\%$. For NWA 5958, $x_{\mathrm{chd}} = 18.9 + 3.6 = 22.5$ vol% (Jacquet et al., 2016), yielding $f_{\mathrm{recycled}} = 12\%$. So debris of earlier chondrules are likely a minority among relicts, and other immediate precursors must be sought.

The Ca-Al-Ti depletion and Mn enrichment of Kaba relict grains relative to their hosts are reminiscent of the minor element characteristics of AOA olivines (Krot et al., 2004; Weisberg et al., 2004; Komatsu et al., 2015). AOA olivines indeed have Ca, Al, Ti contents of 0.15–0.25 wt%, 0.02–0.07 wt% and 0.01–0.05 wt%, respectively, commensurate with those shown by the relicts (Figs. 4–6; Table S1). A subset of them (in the least metamorphosed carbonaceous chondrites only) have Mn contents up to 1.5 wt% (Krot et al., 2004, Schrader et al., 2018), decoupled from Fe, often near the margins of their olivine grains, conform to the progressive Mn-enrichment expected in olivine condensed from a cooling gas of solar composition, or somewhat enriched in dust (Weisberg et al., 2004; Krot et al., 2004; Komatsu et al., 2015, Ebel, 2006). The Fe/Mg ratios of olivine relicts are also similar to those reported for AOA olivines (0–2 mol% fayalite in the least metamorphosed ones, more for the others; (Weisberg et al., 2004; Sugiura et al., 2009; Ruzicka et al., 2012, Krot et al., 2004; Komatsu et al., 2015), even though these are less diagnostic by themselves in comparison to host grains. These mineral chemical affinities are supported by experiments showing that type I chondrules could have derived from the annealing and melting of nebular condensates (Whattam et al., 2008; Whattam and Hewins, 2009). The occasional presence of relict ^{16}O-rich spinels in type I chondrules (Maruyama et al., 1999) may betray AOA material among their precursors. Indeed, AOAs typically contain CAI-like nodules and ribbons mainly composed of spinel, Ti-Ca-rich pyroxene, and anorthite (Weisberg et al., 2004; Sugiura et al., 2009; Ruzicka et al., 2012). Magnesium aluminate spinel commonly observed within AOAs and chondrules has a higher melting temperature than Mg-rich olivine (2135 °C *vs.* 1890 °C). Consequently, they could have been preserved along with olivine relicts, whereas the fusion of other phases with lower melting temperatures during the high-temperature chondrule-forming event(s) may have generated Ca-Al-Ti-rich, but Mn-poor (as Mn is moderately volatile), melts (hereafter CAT melts) similar

to chondrule mesostases (Libourel et al., 2006; Marrocchi and Libourel, 2013). In some cases, unmistakable relict refractory inclusions are found in chondrules, such as a relict AOA in a type II chondrule in CO3.0 chondrite Yamato-81020 (Yurimoto and Wasson, 2002) or relict CAIs in chondrules or chondrule/CAI compound objects in CV (Krot et al., 2007, Aléon & Bourot-Denise, 2008) and CH (Krot et al., 2017) chondrites. Most of the time, though, the only trace of refractory inclusion inheritance may lie in the bulk composition of the chondrule, whether in terms of chemistry (with bulk chondrule REE signatures diagnostic of admixed CAIs (Misawa & and Nakamura, 1988; Jones and Schilk, 2009; Jacquet and Marrocchi, 2017) or isotopic composition, e.g. the ^{50}Ti excesses reported in chondrules from carbonaceous chondrites by (Gerber et al., 2017), which could have inherited part of their Ti from (^{50}Ti-rich) CAI-like material. Thus AOAs are plausible precursors for type I, olivine-rich chondrules.

However, relict olivine grains show more variable Δ^{17}O values than AOA olivines (Krot et al., 2004) and plot between AOA olivines and host grains (Figs. 4–6). Interestingly, relict olivines from Kaba, Murchison, and NWA 5958 plot along the PCM line (Fig. 9; Ushikubo et al., 2012), with CM relicts having less variable and less ^{16}O-enriched compositions than Kaba relicts (Figs. 9, 12B). One could at first envision disturbances during chondrule formation to account for the observed compositional variations. However, the minor element (Mn, Ca, Ti) contents of the relicts vary little with Δ^{17}O and remain in the AOA range (Figs. 4–7). As oxygen diffuses more slowly than those elements (Ryerson et al., 1989; Chakraborty, 2010), chondrule formation does not seem to have affected their contents significantly. Thus, if the precursors were initially as ^{16}O-rich as AOAs, their isotopic exchange with a ^{16}O-poor environment must have occurred before chondrule formation. In fact, AOA olivines themselves in reduced CV chondrites present evidence for such an incipient exchange over timescales of months or years around 1000 °C (Fagan et al., 2004). In addition to time and temperature, a likely control on the extent of this exchange was grain size (i.e., surface/volume ratio). We may envisage chondrule precursors as aggregates similar to present-day CV chondrite matrices, with coarser (supramicron) ^{16}O-rich grains embedded in a finer-grained ^{16}O-poor groundmass as revealed by isotopographs (Kunihiro et al., 2005; Cosarinsky et al., 2008) (see also similar findings on the Kakangari chondrite; Nagashima et al., 2015). As the coarser grains were more likely preserved during chondrule melting, ^{16}O-rich compositions are expected to dominate among relicts, especially in Kaba chondrules. This implies that evolution along the PCM line *predated* chondrule formation.

4.3. Conditions of chondrule formation

To the extent that we may consider that we have disentangled relicts from their hosts, we can now examine the thermal history of chondrule formation itself. As mentioned above, upon partial melting of chondrule precursors, CAT melts were likely generated by the melting of Ca-Al-Ti-rich precursor phases. A fraction of the original olivine may have also experienced dissolution (as the relicts are but a surviving minority), facilitating subsequent olivine saturation in the CAT melt (Soulié et al., 2016). As a result of igneous partitioning with the melt, this later generation of olivine crystallized as Ca-Al-Ti-rich overgrowths around the relicts now found in the chondrule interior.

It is noteworthy that the strong zonings of interior olivines revealed by Al and Ti X-ray maps are much less clear in Ca and Mn maps; likewise relict Fo contents seem to follow those of their hosts, despite significant interchondrule diversity (Figs. 4–7). Al diffuses slowly in natural olivine (Zhukova et al., 2017), and the diffusivity of Ti in olivine is about four orders of magnitude below that of Fe or Ca (Cherniak and Liang, 2014), although (Spandler and O'Neill, 2009) found little difference between the diffusivities of these elements in San Carlos olivine. Given that Mn (whose diffusion coefficient should not be far from that of Ca; Chakraborty, 2010) enrichments survived in some relicts (e.g., Figs. 4–5), the interior olivine grains were likely only marginally homogenized in Ca when the overgrowths grew, and Ca and Mn diffusion coefficients on the order of 10^{-15} m^2/s at olivine crystallization temperatures (Chakraborty, 2010) imply timescales on the order of a day. This of course is only a very rough estimate and dedicated zoning fittings are necessary in the future.

Our SIMS measurements indicate that host olivines present uniform Δ^{17}O values, in contrast to the relicts, indicating buffering by the surrounding gas during chondrule formation. Still, the nature of the main O-bearing molecule that exchanged with chondrule melts remains controversial, however important a constraint on the chondrule-forming event(s) it would be. Most recent models envision interactions with ^{16}O-poor H_2O vapor (Rudraswami et al., 2011; Ushikubo et al., 2012; Schrader et al., 2013, 2014; Tenner et al., 2013, 2015; Hertwig et al., 2018; Chaumard et al., 2018). However, laboratory experiments have shown that chondrule pyroxenes could have formed from the incorporation of SiO from the nebular gas into the chondrule melt (Tissandier et al., 2002). Such a "silicification" process is capable of modifying the bulk chemical and oxygen isotopic compositions of chondrules (Hezel et al., 2006; Libourel et al., 2006; Marrocchi and Libourel, 2013; Marrocchi and Chaussidon, 2015; Friend et al., 2016; Piani et al., 2016). Indeed, since bulk AOA compositions lie on the Si-poor side of the forsterite-anorthite join (Ruzicka et al., 2012), the formation of type I chondrules from AOAs requires an influx of Si from the gas phase (Tissandier et al., 2002; Libourel et al., 2006; Marrocchi and Libourel, 2013; Friend et al., 2016; Piani et al., 2016; Marrocchi et al., 2018a). The outward decreasing Ca, Al, and Ti contents of host olivines indicates that their parental melt underwent dilution (after reaching maximum concentrations at olivine saturation), which can be explained by such an influx of Si and Mg from the gas phase (Libourel and Portail, 2018; Marrocchi et al., 2018a). This may also account for the apparent restriction of relicts to chondrule interiors (as chondrules probably grew outward during their recondensation) as well as the slight drop in Ca content at the edge of interior olivine grains (Figs. 1 and 2; see also Jacquet and Marrocchi, 2017). Such gas-melt interactions under high $P_{SiO(g)}$ would also naturally produce the negative correla-

tion observed between SiO_2 and refractory elements in chondrule mesostases (Libourel et al., 2006). Water vapor alone obviously cannot produce these chemical trends. Of course, both water vapor and gaseous SiO and Mg probably existed in the gas phase phase (Ebel and Grossman, 2000; Komatsu et al., 2018), as is expected in any mixture of solar-composition gas and chondritic dust. Therefore, the host $\Delta^{17}O$ values should roughly represent the average composition of the whole chondrule-forming reservoir (Marrocchi and Chaussidon, 2015), whose different species (condensed or gaseous, but excepting relicts) would have isotopically equilibrated.

The oscillatory Al and Ti zonings (but not Ca and Mn, again probably because of their higher diffusivities) of the large (subhedral) outer-chondrule olivine crystals are intriguing (Fig. 3). They are reminiscent of isolated olivine grains observed in chondrite matrices (Steele, 1995), suggesting that such isolated olivine crystals are fragments from olivine-rich chondrules. Such zonings may be related to the oscillatory zonings described for pyroxene in several chondrules (Jones, 1996; Baecker et al., 2017); indeed, the formation of outer-chondrule olivine and pyroxene (concentrated near the margin) was probably spatially and temporally close, and although we focused on olivine-rich chondrules, an oscillatorily zoned, euhedral enstatite phenocryst is visible in Fig. 1. Baecker et al. (2017) ascribed their pyroxene zoning to dissolution/precipitation cycles induced by multiple secondary heating of the mesostasis, but notwithstanding the requirement for an excessive frequency of chondrule-forming events (Jacquet et al., 2015), this would be hardly applicable for palisadic olivine given that the oscillations only appear on one side. Another possibility would be a boundary layer effect, similar to that envisioned by (Jones, 1996). A third possibility would be an analogy with the dendritic P, Al, and Cr zonings commonly observed in terrestrial, lunar, and Martian olivine crystals and interpreted as evidence of fast, diffusion-controlled growth at high supersaturation (Welsch et al., 2014). However, while some sections of such crystals would resemble the zonings found here, one would also expect feathery patterns (Welsch et al., 2014) not observed in this work. This would suggest slow growth rates of palisadic olivine at low supersaturation due to variations in melt temperature (cooling rates less than a few 100 K/h) and/or composition, which must have been moderate and persistent enough to allow crystallization of large, nondendritic, olivine crystals (Faure et al., 2003). If we combine this with the cooling rates of order 250–10,000 K/h suggested by the widespread monoclinic structure of enstatite in type I chondrules (Soulié et al., 2016), this may indicate that the late phase of chondrule growth recorded by the outer parts of chondrules (large palisadic olivine and rimming pyroxene) lasted on the order of an hour. At any rate, the exact origin of the oscillatory of outer chondrule olivine remains unclear and its identification may have to await experimental simulations.

4.4. Cosmochemical implications

The genetic link between AOAs and type I chondrules suggested by this study (summarized in Fig. 13) raises the question of the timing of chondrule formation during the evolution of the SPD. The ^{26}Al-^{26}Mg systematics of bulk chondrules limit the formation of chondrule precursors to the first 1.5 Myr after the formation of CAIs (Luu et al., 2015). This is consistent with AOA condensation within the hot (>1000–1500 K) zone of the SPD that extended from a few tenths to ~1 AU (Faure et al., 2014). In-situ ^{26}Al-^{26}Mg and bulk chondrule Pb-Pb dating show that chondrule formation (i.e., the last melting events) began during the formation of CAIs and AOAs, and lasted up to 4 Myr (Connelly et al., 2012; Luu et al., 2015). In addition, the initial Pb isotopic compositions of chondrules that crystallized >1 Myr after solar system formation suggest that chondrules were formed by recycling of volatile-depleted precursors (Bollard et al., 2017) such as AOAs or first generations of chondrules. These arguments imply either that the energy source for melting chondrule precursors was in the vicinity of the condensation zone or that AOAs experienced efficient transport in the SPD (Jacquet et al., 2012).

The ^{16}O-rich composition of AOAs compared to chondrules indicates that they interacted with a gaseous reservoir that was $^{17,18}O$-enriched relative to their condensation zones (Fig. 13). Such a reservoir could have been produced by the inward migration of ^{16}O-poor ice/-dust from the outer disk (Yurimoto and Kuramoto, 2004), probably later than refractory-inclusion formation since numerous CAIs and their Wark-Lovering rims have homogeneous ^{16}O-rich compositions (Bodénan et al., 2014), despite some variation (e.g., Kawasaki et al., 2017; Aléon, 2018). We have insufficient data to discuss whether the thermal events that led to these partial equilibrations of chondrule precursors with their environment were related to neighboring chondrule-forming events, though we argued in Section 4.2 that the O isotopic evolution of chondrule precursors along the PCM line probably predated most chondrules.

The fact that chondrule precursors seem more ^{16}O-rich in Kaba than in C2 chondrites (mean relict $\Delta^{17}O$ values of -9.4 ± 0.8 and -5.6 ± 0.7‰, respectively; the quoted uncertainty here and henceforth being the standard error of the mean) is consistent with the larger abundance of refractory inclusions in CV than in CM chondrites (e.g., Hezel et al., 2008) in the sense that the CV reservoir included a larger contribution of components formed in the ^{16}O-rich refractory inclusion-forming region. Yet, the mean $\Delta^{17}O$ values of *host* type I chondrules show little variation between carbonaceous chondrite groups: -5.2 ± 0.2‰ for Kaba (CV3; Hertwig et al., 2018; -4.8 ± 0.3‰ for Murchison CM2; Chaumard et al., 2018; -5.2 ± 0.2‰ for Yamato 81020 CO3; Tenner et al., 2013; and -4.7 ± 0.4‰ for Acfer 094 C2-ung; Ushikubo et al., 2012). CRs are the exception with -2.8 ± 0.2‰ (Tenner et al., 2015). Since the host-chondrule O isotopic composition should have been buffered by that of their native region, this suggests that the ^{16}O-poor component, whatever its nature (ice, dust; Ebel et al., 2018), was fairly evenly distributed across carbonaceous chondrite reservoirs by the time most of their chondrules formed. However, given the interchondrule $\Delta^{17}O$ variations (even among type Is) in sin-

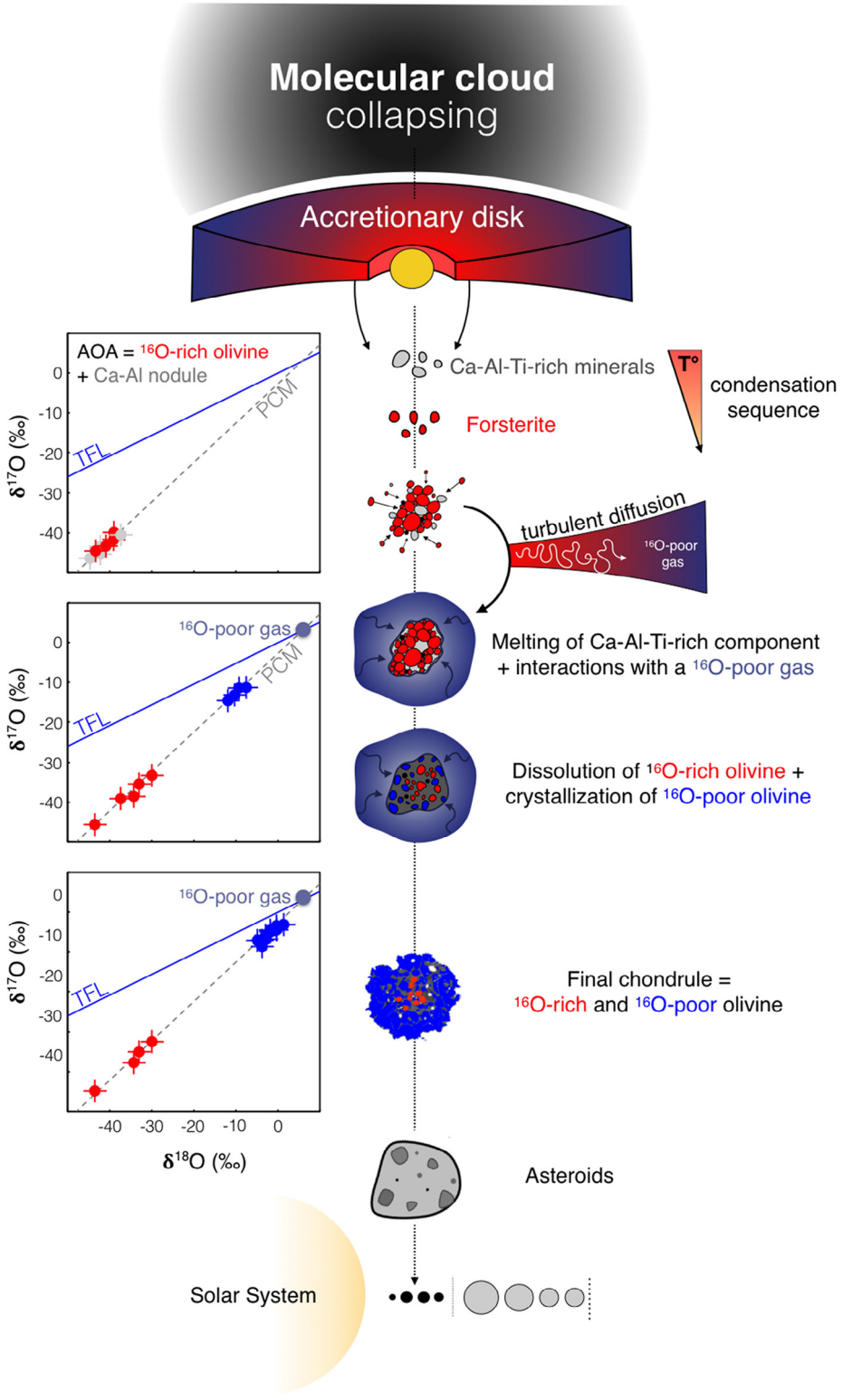

Fig. 13. Schematic representation of chondrule formation. Previously condensed ^{16}O-rich AOAs are transported towards ^{17,18}O-rich zones of the disk due to turbulent diffusion. They experienced melting and massive gas-melt interactions, inducing melting of AOA-inherited Ti-Al-Ca-rich components, dissolution of ^{16}O-rich relict olivines (red) and crystallization of Ti-Al-Ca-rich and ^{16}O-poor olivines (blue). The final chondrules thus comprise AOA-inherited ^{16}O-rich relict olivines and ^{17,18}O-rich olivines that recrystallized as new grains or overgrowths during gas-melt interactions.

gle chondrites, local variations of the proportions between ^{16}O-rich and -poor endmembers did occur in each reservoir, possibly as a result of variable solid/gas ratios (e.g., Schrader et al., 2013; Tenner et al., 2015; Marrocchi and Chaussidon, 2015; Tenner et al., 2018) and/or changes in the pre-chondrule-heating state of water (ice or vapor, depending on the position of the snow line and whether water correlates with chondritic dust). The different frequencies of chondrule-forming events (and thus variable fractions of precursor materials subject to isotopic equilibration with more labile phases such as ices) in the different carbonaceous chondrite reservoirs, as well as the heterogeneous (re)distribution of ^{16}O-poor water in chondrite parent bodies (Clayton and Mayeda, 1999; Vacher et al., 2016; Verdier-Paoletti et al., 2017; Fujiya, 2018; Marrocchi et al., 2018b), may have further contributed to the observed bulk oxygen isotopic variations among carbonaceous chondrites.

5. CONCLUDING REMARKS

We have combined *in situ* EMPA elemental and SIMS oxygen isotopic analyses of porphyritic olivine-rich chondrules in Kaba (CV3) after characterization by X-ray mapping. Our main results are:

1. Porphyritic olivine-rich chondrules show complex textures with clear chemical zoning between chondrule cores, characterized by small Ca-Al-Ti-poor and Mn-rich olivine grains, and exteriors, containing larger Ca-Al-Ti-rich and Mn-poor olivine crystals.
2. The enrichment in refractory elements decreases drastically in the outermost parts of chondrules, which show complex oscillatory Al and Ti zonings.
3. Relict olivines grains, defined as those with Δ^{17}O values beyond 3σ of the host value, are systematically Al-Ti-poor and Mn-rich, whereas host grains show variable minor element abundances and relatively constant Δ^{17}O values.

From these observations, we propose the following interpretations:

1. The chemical zonings and non-refractory nature of relict grains with mass-independent O isotopic variations relative to their hosts do not support a chondrule origin via crystallization of condensed refractory melts as recently proposed (Libourel and Portail, 2018).
2. Chemical and O isotopic features support a genetic link between AOAs and chondrules, although relict olivine grains show a larger range of Δ^{17}O values than AOA olivines.
3. Chondrules formed by incomplete melting of isotopically heterogeneous nebular condensates comprising Ca-Al-Ti-poor and Mn-rich relict olivine grains, Fe-Ni metal beads, and Ca-Al-Ti-rich minerals (e.g., anorthite, clinopyroxene). Melting of the latter produced Ca-Al-Ti-rich melts (CAT melts) and induced the partial dissolution of relict olivine grains inherited from AOAs.
4. Incoming Mg and Si from the gas phase sustained the subsequent crystallization of host olivine crystals from CAT melts by gas-assisted epitaxial growth on relict olivine grains. Host olivine grains are characterized by (i) a higher concentration of refractory elements (i.e., Ti, Al and Ca) than relicts, in agreement with olivine/melt partition coefficients, (ii) lower Mn concentrations than relicts due to a dilution effect (CAT melts being depleted in Mn), and (iii) relatively constant Δ^{17}O values.
5. Protracted gas–melt interactions induced CAT melt dilution, counteracting the enrichment of refractory elements due to olivine crystallization and producing oscillatory zonings at chondrule edges.
6. The O isotopic characteristics and zoning patterns of chondrule olivine crystals reveal complex nebular histories that are difficult to reconcile with models of monotonic cooling in isotopically homogeneous melts.
7. Together, these results indicate a genetic link between AOA-like condensates and type I chondrules, implying that dust recycling was a major process in the early Solar System.

ACKNOWLEDGEMENTS

All data used in the present article are available by contacting Yves Marrocchi. Laurette Piani, David Bekaert, Michel Fialin, Nicolas Rividi, Andrey Gurenko, Laurent Tissandier, François Faure, Guy Libourel and Mathieu Roskosz are thanked for helpful scientific and technical discussions. Nordine Bouden is thanked for his assistance with isotopic measurements. Devin Schrader, Tim Fagan and Noriuyki Kawasaki are thanked for constructive comments and Associate Editor Sara Russell for careful editing. This is CRPG-CNRS contribution #2602.

APPENDIX A. SUPPLEMENTARY MATERIAL

Supplementary data to this article can be found online at https://doi.org/10.1016/j.gca.2018.12.038.

REFERENCES

Aléon J. and Bourot-Denise M. (2008) Mineralogy and petrography of a spectacular refractory inclusion that underwent chondrule formation. *39th Lunar and Planetary Science Conference, Houston, USA*.

Aléon J. (2018) Closed system oxygen isotope redistribution in igneous CAIs upon spinel dissolution. *Earth Planet. Sci. Lett.* **482**, 324–333.

Baecker B., Rubin A. E. and Wasson J. T. (2017) Secondary melting events in Semarkona chondrules revealed by compositional zoning in low-Ca pyroxene. *Geochim. Cosmochim. Acta* **211**, 256–279.

Batanova V. G., Sobolev A. V. and Kuzmin D. V. (2015) Trace element analysis of olivine: High precision analytical method for JEOL JXA-8230 electron probe microanalyser. *Chem. Geol.* **419**, 149–157.

Bodénan J.-D., Starkey N. A., Russell S. S., Wright I. P. and Franchi I. A. (2014) An oxygen isotope study of Wark-Lovering rims on type A CAIs in primitive carbonaceous chondrites. *Earth Planet. Sci. Lett.* **401**, 327–336.

Bollard J., Connelly J. N., Whitehouse M. J., Pringle E. A., Bonal L., Jørgensen J. K., Nordlund Å., Moynier F. and Bizzarro M. (2017) Early formation of planetary building blocks inferred from Pb isotopic ages of chondrules. *Sci. Adv.* **3**, e1700407.

Bonal L., Quirico E., Bourot-Denise M. and Montagnac G. (2006) Determination of the petrologic type of CV3 chondrites by Raman spectroscopy of included organic matter. *Geochim. Cosmochim. Acta* **70**, 1849–1863.

Campbell A. J., Zanda B., Perron C., Meibom A. and Petaev M. I. (2005) Origin and thermal history of Fe-Ni metal in primitive chondrites. *Chondrites and the Protoplanetary Disk. ASP Conference Series* **vol. 341**, p. 286.

Chakraborty S. (2010) Diffusion coefficients in Olivine, Wadsleyite and Ringwoodite. *Rev. Mineral. Geochem.* **72**, 603–639.

Chaumard N. L., Defouilloy C. and Kita N. T. (2018) Oxygen isotope systematics of chondrules in the Murchison CM2 chondrite and implications for the CO-CM relationship. *Geochim. Cosmochim. Acta* **228**, 220–242.

Cherniak D. J. and Liang Y. (2014) Titanium diffusion in olivine. *Geochim. Cosmochim. Acta* **147**, 43–57.

Clayton R. N. and Mayeda T. K. (1999) Oxygen isotope studies of carbonaceous chondrites. *Geochim. Cosmochim. Acta* **63**, 2089–2104.

Cohen B. A., Hewins R. H. and Alexander C. M. O. (2004) The formation of chondrules by open-system melting of nebular condensates. *Geochim. Cosmochim. Acta* **68**, 1661–1675.

Connelly J. N., Bizzarro M., Krot A. N. and Nordlund A. (2012) The absolute chronology and thermal processing of solids in the solar protoplanetary disk. *Science* **338**, 651–655.

Connolly H. C. and Jones R. H. (2016) Chondrules: the canonical and noncanonical views. *J. Geophys. Res. Planets* **121**, 1885–1899.

Cosarinsky M., Leshin L. A., MacPherson G. J., Guan Y. and Krot A. N. (2008) Chemical and oxygen isotopic compositions of accretionary rim and matrix olivine in CV chondrites: constraints on the evolution of nebular dust Geochim. *Cosmochim. Acta* **72**, 1887–1913.

Ebel D. S. and Grossman L. (2000) Condensation in dust-enriched systems. *Geochim. Cosmochim. Acta* **64**, 339–366.

Ebel D. S. (2006) Condensation of rocky material in astrophysical environments. In *Meteorites and the Early Solar System II* (eds. D. S. Lauretta and H. Y. McSween). University of Arizona Press, Tucson, pp. 253–277, 943 pp.

Ebel D. S., Brunner C., Konrad K., Leftwich K., Erb I., Lu M., Rodriguez H., Crapster-Pregont E. J., Friedrich J. M. and Weisberg M. K. (2016) Abundance, major element composition and size of components and matrix in CV, CO and Acfer 094 chondrites. *Geochim. Cosmochim. Acta* **172**, 322–356.

Ebel D. S., Alexander C. M. O. and Libourel G. (2018) Vapor–melt exchange. In *Chondrules*. Cambridge University Press, pp. 151–174, 441 pp.

Fagan T. J., Krot A. N., Keil K. and Yurimoto H. (2004) Oxygen isotopic evolution of amoeboid olivine aggregates in the reduced CV3 chondrites Efremovka Vigarano, and Leoville. *Geochim. Cosmochim. Acta* **68**, 2591–2611.

Faure F., Trolliard G., Nicollet C. and Montel J.-M. (2003) A developmental model of olivine morphology as a function of the cooling rate and the degree of undercooling. *Contrib. Mineral. Petrol.* **145**, 251–263.

Faure J., Fromang S. and Latter H. (2014) Thermodynamics of the dead-zone inner edge in protoplanetary disks. *A&A* **564**, A22–A116.

Friend P., Hezel D. C. and Mucerschi D. (2016) The conditions of chondrule formation, Part II: Open system. *Geochim. Cosmochim. Acta* **173**, 198–209.

Fujiya W. (2018) Oxygen isotopic ratios of primordial water in carbonaceous chondrites. *Earth Planet. Sci. Lett.* **481**, 264–272.

Gerber S., Burkhardt C., Budde G., Metzler K. and Kleine T. (2017) Mixing and transport of dust in the early solar nebula as inferred from titanium isotope variations among chondrules. *Astrophys. J. Lett.* **841**, L17.

Gooding J. L. and Keil K. (1981) Relative abundances of chondrule primary textural types in ordinary chondrites and their bearing on conditions of chondrule formation. *Meteorit. Planet. Sci.* **16**, 17–43.

Grossman J. N. and Wasson J. T. (1985) The origin and history of the metal and sulfide components of chondrules. *Geochim. Cosmochim. Acta* **49**, 925–939.

Hertwig A. T., Defouilloy C. and Kita N. T. (2018) Formation of chondrules in a moderately high dust enriched disk: evidence from oxygen isotopes of chondrules from the Kaba CV3 chondrite. *Geochim. Cosmochim. Acta* **224**, 116–131.

Hewins R. H., Connolly H. C., Logfren G. E. J. and Libourel G. (2005) Experimental constraints on chondrules formation. In *Chondrites and the Protoplanetary Disk. ASP Conference Series*, vol. 341 (eds. Alexander N. Krot, Edward R. D. Scott and B Reipurth). Astronomical Society of the Pacific, San Francisco, p. 286.

Hezel D. C., Palme H., Nasdala L. and Brenker F. E. (2006) Origin of SiO_2-rich components in ordinary chondrites. *Geochim. Cosmochim. Acta* **70**, 1548–1564.

Hezel D. C., Russell S. S., Ross A. J. and Kearsley A. T. (2008) Modal abundances of CAIs: implications for bulk chondrite element abundances and fractionations. *Meteorit. Planet. Sci.* **43**, 1879–1894.

Jacquet E. and Marrocchi Y. (2017) Chondrule heritage and thermal histories from trace element and oxygen isotope analyses of chondrules and amoeboid olivine aggregates. *Meteorit. Planet. Sci.* **52**, 2672–2694.

Jacquet E., Alard O. and Gounelle M. (2015) Trace element geochemistry of ordinary chondrite chondrules: the type I/type II chondrule dichotomy. *Geochim. Cosmochim. Acta* **155**, 47–67.

Jacquet E., Barrat J.-A., Beck P., Caste F., Gattacceca J., Sonzogni C. and Gounelle M. (2016) Northwest Africa 5958: A weakly altered CM-related ungrouped chondrite, not a CI3. *Meteorit. Planet. Sci.* **51**, 851–869.

Jacquet E., Gounelle M. and Fromang S. (2012) On the aerodynamic redistribution of chondrite components in protoplanetary disks. *Icarus* **220**, 162–173.

Jacquet E., Paulhiac-Pison M., Alard O., Kearsley A. T. and Gounelle M. (2013) Trace element geochemistry of CR chondrite metal. *Meteorit. Planet. Sci.* **48**, 1981–1999.

Jones R. H. (1996) FeO-rich, porphyritic pyroxene chondrules in unequilibrated ordinary chondrites. *Geochim. Cosmochim. Acta* **60**, 3115–3138.

Jones R. H., Leshin L. A., Guan Y. and Sharp Z. D. (2004) Oxygen isotope heterogeneity in chondrules from the Mokoia CV3 carbonaceous chondrite. *Geochim. Cosmochim. Acta* **68**, 3423–3438.

Jones R. H. and Schilk A. J. (2009) Chemistry, petrology and bulk oxygen isotope compositions of chondrules from the Mokoia CV3 carbonaceous chondrite. *Geochim. Cosmochim. Acta* **73**, 5854–5883.

Kawasaki N., Itoh S., Sakamoto N. and Yurimoto H. (2017) Chronological study of oxygen isotope composition for the solar protoplanetary disk recorded in a fluffy Type A CAI from Vigarano. *Geochim. Cosmochim. Acta* **201**, 83–102.

Komatsu M., Fagan T. J., Krot A. N., Nagashima K., Petaev M. I., Kimura M. and Yamaguchi A. (2018) First evidence for

silica condensation within the solar protoplanetary disk. *PNAS* **1**, 201722265–201722266.

Komatsu M., Fagan T. J., Mikouchi T., Petaev M. I. and Zolensky M. E. (2015) LIME silicates in amoeboid olivine aggregates in carbonaceous chondrites: Indicator of nebular and asteroidal processes. *Meteorit. Planet. Sci.* **50**, 1271–1294.

Krot A. N., Petaev M. I., Russell S. S., Itoh S., Fagan T. J., Yurimoto H., Chizmadia L., Weisberg M. K., Komatsu M., Ulyanov A. A. and Keil K. (2004) Amoeboid olivine aggregates and related objects in carbonaceous chondrites: records of nebular and asteroid processes. *Chemie der Erde – Geochem.* **64**, 185–239.

Krot A. N., Yurimoto H., Hutcheon I. D., Chaussidon M., MacPherson G. J. and Paque J. (2007) Remelting of refractory inclusions in the chondrule-forming regions: Evidence from chondrule-bearing type C calcium-aluminum-rich inclusions from Allende. *Meteorit. Planet. Sci.* **42**, 1197–1219.

Krot A. N., Nagashima K., van Kooten E. M. M. and Bizzarro M. (2017) Calcium–aluminum-rich inclusions recycled during formation of porphyritic chondrules from CH carbonaceous chondrites. *Geochim. Cosmochim. Acta.* **201**, 185–223.

Kunihiro T., Nagashima K. and Yurimoto H. (2005) Microscopic oxygen isotopic homogeneity/heterogeneity in the matrix of the Vigarano CV3 chondrite. *Geochim. Cosmochim. Acta* **69**, 763–773.

Libourel G. and Krot A. N. (2007) Evidence for the presence of planetesimal material among the precursors of magnesian chondrules of nebular origin. *Earth Planet. Sci. Lett.* **254**, 1–8.

Libourel G. and Portail M. (2018) Chondrules as direct thermochemical sensors of solar protoplanetary disk gas. *Sci. Adv.* **4**, eaar3321.

Libourel G., Krot A. and Tissandier L. (2006) Role of gas-melt interaction during chondrule formation. *Earth Planet. Sci. Lett.* **251**, 232–240.

Lusby D., Scott E. R. D. and Keil K. (1987) Ubiquitous high-FeO silicates in enstatite chondrites. *J. Geophys. Res.* **92**, E679–E695.

Luu T.-H., Young E. D., Gounelle M. and Chaussidon M. (2015) Short time interval for condensation of high-temperature silicates in the solar accretion disk. *PNAS* **112**, 1298–1303.

Marrocchi Y. and Chaussidon M. (2015) A systematic for oxygen isotopic variation in meteoritic chondrules. *Earth Planet. Sci. Lett.* **430**, 308–315.

Marrocchi Y., Chaussidon M., Piani L. and Libourel G. (2016) Early scattering of the solar protoplanetary disk recorded in meteoritic chondrules. *Sci. Adv.* **2**, e1601001–e1601001.

Marrocchi Y. and Libourel G. (2013) Sulfur and sulfides in chondrules. *Geochim. Cosmochim. Acta* **119**, 117–136.

Marrocchi Y., Villeneuve J., Batanova V., Piani L. and Jacquet E. (2018a) Oxygen isotopic diversity of chondrule precursors and the nebular origin of chondrules. *Earth Planet. Sci. Lett.* **496**, 132–141.

Marrocchi Y., Bekaert D. V. and Piani L. (2018b) Origin and abundance of water in carbonaceous asteroids. *Earth Planet. Sci. Lett.* **482**, 23–32.

Maruyama S., Yurimoto H. and Sueno S. (1999) Oxygen isotope evidence regarding the formation of spinel-bearing chondrules. *Earth Planet. Sci. Lett.* **169**, 165–171.

McCanta M. C., Beckett J. R. and Stolper E. M. (2016) Correlations and zoning patterns of phosphorus and chromium in olivine from H chondrites and the LL chondrite Semarkona. *Meteorit. Planet. Sci.* **51**, 520–546.

Misawa K. and Nakamura N. (1988) Highly fractionated rare-earth elements in ferromagnesian chondrules from the Felix (CO_3) meteorite. *Nature* **334**, 47–50.

Nagashima K., Krot A. N. and Huss G. R. (2015) Oxygen-isotope compositions of chondrule phenocrysts and matrix grains in Kakangari K-grouplet chondrite: implication to a chondrule-matrix genetic relationship. *Geochim. Cosmochim. Acta* **151**, 49–67.

Pack A., Palme H. and Shelley J. M. G. (2005) Origin of chondritic forsterite grains. *Geochim. Cosmochim. Acta* **69**, 3159–3182.

Pack A., Yurimoto H. and Palme H. (2004) Petrographic and oxygen-isotopic study of refractory forsterites from R-chondrite Dar al Gani 013 (R3.5–6), unequilibrated ordinary and carbonaceous chondrites. *Geochim. Cosmochim. Acta* **68**, 1135–1157.

Piani L., Marrocchi Y., Libourel G. and Tissandier L. (2016) Magmatic sulfides in the porphyritic chondrules of EH enstatite chondrites. *Geochim. Cosmochim. Acta* **195**, 84–99.

Rudraswami N. G., Ushikubo T., Nakashima D. and Kita N. T. (2011) Oxygen isotope systematics of chondrules in the Allende CV3 chondrite: High precision ion microprobe studies. *Geochim. Cosmochim. Acta* **75**, 7596–7611.

Russell S. S., Krot A. N., Huss G. R., Keil K., Itoh S., Yurimoto H. and MacPherson G. J. (2005) The genetic relationship between refractory inclusions and chondrules. In *Chondrites and the Protoplanetary Disk. ASP Conference Series*, vol. 341 (eds. Alexander N. Krot, Edward R. D. Scott and B Reipurth). Astronomical Society of the Pacific, San Francisco, p. 317.

Ruzicka A., Floss C. and Hutson M. (2012) Amoeboid olivine aggregates (AOAs) in the Efremovka, Leoville and Vigarano (CV3) chondrites: a record of condensate evolution in the solar nebula. *Geochim. Cosmochim. Acta* **79**, 79–105.

Ruzicka A., Hiyagon H., Hutson M. and Floss C. (2007) Relict olivine, chondrule recycling, and the evolution of nebular oxygen reservoirs. *Earth Planet. Sci. Lett.* **257**, 274–289.

Ryerson F. J., Durham W. B., Cherniak D. J. and Lanford W. A. (1989) Oxygen diffusion in olivine: Effect of oxygen fugacity and implications for creep. *J. Geophys. Res.* **94**, 4105–4118.

Schrader D. L., Connolly, Jr., H. C., Lauretta D. S., Nagashima K., Huss G. R., Davidson J. and Domanik K. J. (2013) The formation and alteration of the Renazzo-like carbonaceous chondrites II: Linking O-isotope composition and oxidation state of chondrule olivine. *Geochim. Cosmochim. Acta* **101**, 302–327.

Schrader D. L., Nagashima K., Krot A. N., Ogliore R. C. and Hellebrand E. (2014) Variations in the O-isotope composition of gas during the formation of chondrules from the CR chondrites. *Geochim. Cosmochim. Acta* **132**, 50–74.

Schrader D. L., Nagashima K., Krot A. N., Ogliore R. C., Yin Q.-Z., Amelin Y., Stirling C. H. and Kaltenbach A. (2017) Distribution of 26Al in the CR chondrite chondrule-forming region of the protoplanetary disk. *Geochim. Cosmochim. Acta* **201**, 275–302.

Schrader D. L., Nagashima K., Waitukaitis S. R., Davidson J., McCoy T. J., Connolly H. C. and Lauretta D. S. (2018) The retention of dust in protoplanetary disks: evidence from agglomeratic olivine chondrules from the outer solar system. *Geochim. Cosmochim. Acta* **223**, 405–421.

Scott E. R. D. and Krot A. N. (2014) *Chondrites and Their Components, Meteorites and Cosmochemical Processes, Volume 1 of Treatise on Geochemistry*, second ed. Elsevier, pp. 65–137.

Soulié C., Libourel G. and Tissandier L. (2016) Olivine dissolution in molten silicates: an experimental study with application to chondrule formation. *Meteorit. Planet. Sci.* **52**, 225–250.

Spandler C. and O'Neill H. S. C. (2009) Diffusion and partition coefficients of minor and trace elements in San Carlos olivine at 1300°C with some geochemical implications. *Contrib. Mineral. Petrol.* **159**, 791–818.

Steele I. M. (1986) Compositions and textures of relic forsterite in carbonaceous and unequilibrated ordinary chondrites. *Geochim. Cosmochim. Acta* **50**, 1379–1395.

Steele I. M. (1995) Oscillatory zoning in meteoritic forsterite. *Am. Mineral.* **80**, 823–832.

Steele I. M., Smith J. V. and Skirius C. (1985) Cathodoluminescence zoning and minor elements in forsterites from the Murchison (C2) and Allende (C3V) carbonaceous chondrites. *Nature* **313**, 294–297.

Sugiura N., Petaev M. I., Kimura M., Miyazaki A. and Hiyagon H. (2009) Nebular history of amoeboid olivine aggregates. *Meteorit. Planet. Sci.* **44**, 559–572.

Tenner T. J., Nakashima D., Ushikubo T., Kita N. T. and Weisberg M. K. (2015) Oxygen isotope ratios of FeO-poor chondrules in CR3 chondrites: influence of dust enrichment and H_2O during chondrule formation. *Geochim. Cosmochim. Acta* **148**, 228–250.

Tenner T. J., Ushikubo T., Kurahashi E., Kita N. T. and Nagahara H. (2013) Oxygen isotope systematics of chondrule phenocrysts from the CO3.0 chondrite Yamato 81020: evidence for two distinct oxygen isotope reservoirs. *Geochim. Cosmochim. Acta* **102**, 226–245.

Tenner T. J., Ushikubo T., Nakashima D., Schrader D. L., Weisberg M. K., Kimura M. and Kita N. T. (2018) Oxygen isotope characteristics of chondrules from recent studies by secondary ion mass spectrometry. In *Chondrules*. Cambridge University Press, pp. 196–246, 441 pp.

Tissandier L., Libourel G. and Robert F. (2002) Gas-melt interactions and their bearing on chondrule formation. *Meteorit. Planet. Sci.* **37**, 1377–1389.

Ushikubo T., Kimura M., Kita N. T. and Valley J. W. (2012) Primordial oxygen isotope reservoirs of the solar nebula recorded in chondrules in Acfer 094 carbonaceous chondrite. *Geochim. Cosmochim. Acta* **90**, 242–264.

Vacher L. G., Marrocchi Y., Verdier-Paoletti M., Villeneuve J. and Gounelle M. (2016) Inward radial mixing of interstellar water ices in the solar protoplan-etary disk. *Astrophys. J. Lett.* **826**, 1–6.

Verdier-Paoletti M. J., Marrocchi Y., Avice G., Roskosz M., Gurenko A. and Gounelle M. (2017) Oxy-gen isotope constraints on the alteration temperatures of CM chondrites. *Earth Planet. Sci. Lett.* **458**, 273–281.

Weisberg M. K., Connolly H. C. and Ebel D. S. (2004) Petrology and origin of amoeboid olivine aggregates in CR chondrites. *Meteorit. Planet. Sci.* **39**, 1741–1753.

Welsch B., Hammer J. and Hellebrand E. (2014) Phosphorus zoning reveals dendritic architecture of olivine. *Geology* **42**, 867–870.

Whattam S. A. and Hewins R. H. (2009) Granoblastic olivine aggregates as precursors of Type I chondrules: an experimental test. *Geochim. Cosmochim. Acta* **73**, 5460–5482.

Whattam S. A., Hewins R. H., Cohen B. A., Seaton N. C. and Prior D. J. (2008) Granoblastic olivine aggregates in magnesian chondrules: planetesimal fragments or thermally annealed solar nebula condensates? *Earth Planet. Sci. Lett.* **269**, 200–211.

Yurimoto H. and Kuramoto K. (2004) Molecular cloud origin for the oxygen isotope heterogeneity in the solar system. *Science* **305**, 1763–1766.

Yurimoto H. and Wasson J. T. (2002) Extremely rapid cooling of a carbonaceous-chondrite chondrule containing very O-rich olivine and a ^{26}Mg-excess. *Geochim. Cosmochim. Acta* **66**, 4355–4363.

Zanda B., Hewins R., Bourot-Denise M., Bland P. and Albarede F. (2006) Formation of solar nebula reservoirs by mixing chondritic components. *Earth Planet. Sci. Lett.* **248**, 650–660.

Zhukova I., O'Neill H. and Campbell I. H. (2017) A subsidiary fast-diffusing substitution mechanism of Al in forsterite investigated using diffusion experiments under controlled thermodynamic conditions. *Contrib. Mineral. Petrol.* **172**, 1–12.